H1 note H1-01/03-607 Version of 15/1/2003

Further Report on the Beam-Induced Backgrounds in the H1 Detector

H1 background working group

V. Andreev, W. Bartel, J. Bracinik, A. Buniatian, E. Elsen, R. Felst, J. Ferencei, P. Fleischmann, J. Gayler, K. Gadow, S. Gorbounov, T. Greenshaw, H. Henschel, M. Kapishin, M. Klein, C. Kleinwort, P. Kostka, J. Kretzschmar, V. Lendermann, S. Levonian, B. List, R. Lopez-Fernandez, L. Lytkin, N. Malden, T. Naumann, C. Niebuhr, M. Nozicka, D. Pitzl, E. Rizvi, J. Schaffran, A. Schöning, H.-C. Schultz-Coulon, A. Specka, R. Stamen, F. Tomasz, I. Tsurin, P. Van Mechelen, K. Wacker.

Abstract

HERA running in the last quarter of 2002 is described, as is the developing understanding of the beam-induced backgrounds in the H1 detector. Comparisons are presented of the sensitivity of H1 to proton-induced background before and after the luminosity upgrade as well as of the residual gas composition and pressure in the H1 vacuum chamber. The backgrounds in the H1 central chambers are discussed and their dependence on the HERA beam currents and running conditions investigated. Various studies are described which were designed to localise the source of the positron beam induced outgassing responsible for the poor vacuum during HERA operation. Finally, proposed further studies and measures designed to combat the H1 background problems are presented.

Contents

1 Introduction

Since the HERA II luminosity upgrade, performed in 2001/2002, the operation of the H1 detector has been hindered by large beam-induced backgrounds as is discussed in detail in a previous report [1], released in October 2002. This document describes the HERA running since that time from an H1 perspective and discusses the developments in the background situation. Familiarity with the HERA machine, the H1 detector and the observed background problems, as described in [1], is assumed in the following.

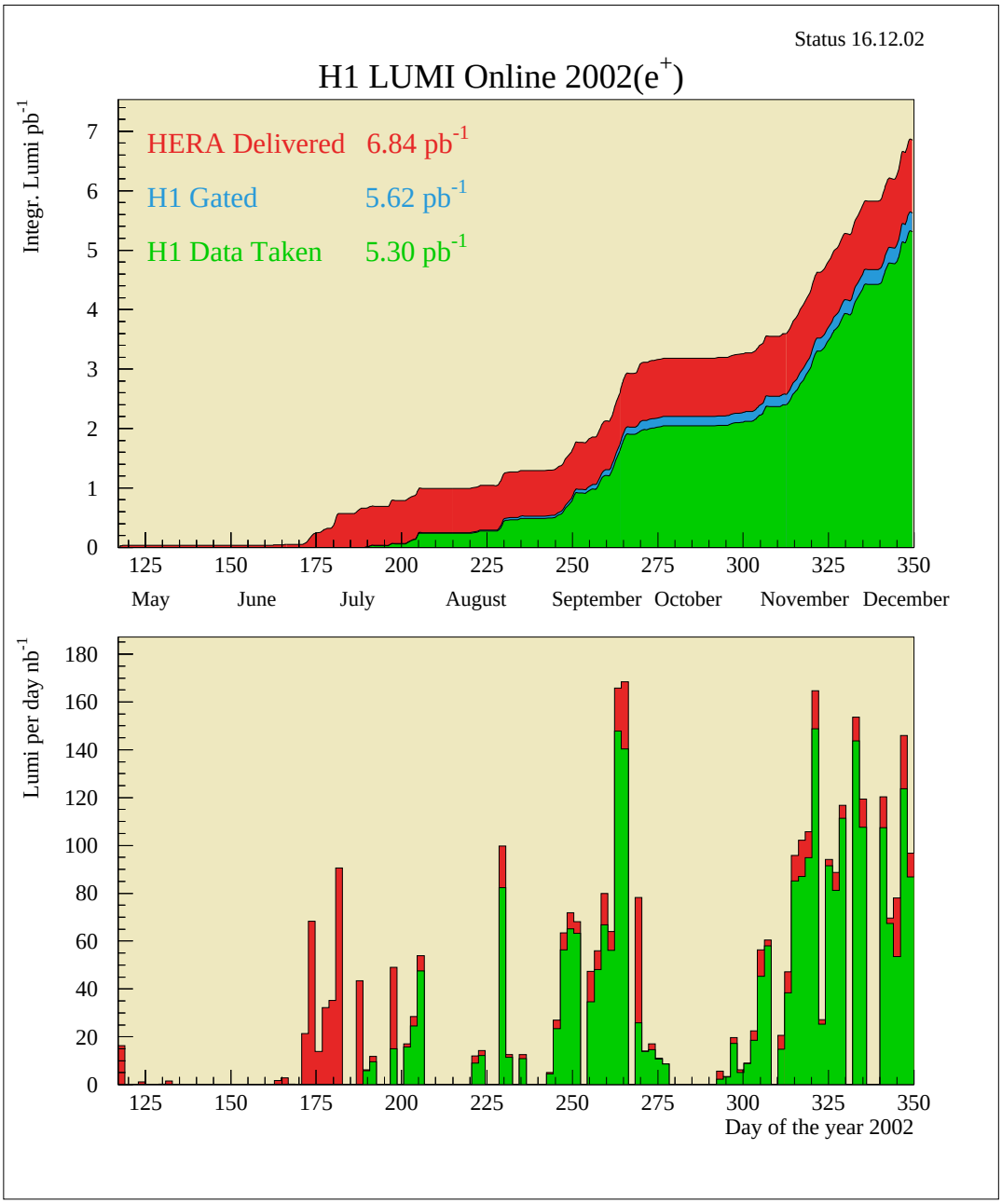

Figure 1: The integrated (top) and daily (bottom) luminosity recorded by the H1 experiment in 2002.

1.1 Recent H1 running

Figure 1 illustrates the luminosity accumulated by H1 during 2002. During the last quarter of the year, HERA delivered a luminosity of about $4.6\,\mathrm{pb}^{-1}$, largely during a relatively small number of runs in which the machine operated smoothly. Overall H1 data taking efficiency exceeded 90% during this period, but unfortunately the background situation only allowed operation of the central jet chambers (CJC1 and CJC2) during about 40% of the data taking. Problematic were both the continuous current drawn in the chambers and sharp background spikes which caused trips. Nonetheless, the data provided first indications of the potential of HERA II, as is illustrated by the extremely high Q^2 event depicted in figure 2 which was recorded during this period. They are being used in searches for new physics at high Q^2 as well as for commissioning and calibrating the many new components of H1 that were introduced during the upgrade. The accumulation of the largest possible data sample before the shut down in early March 2003 is therefore desirable.

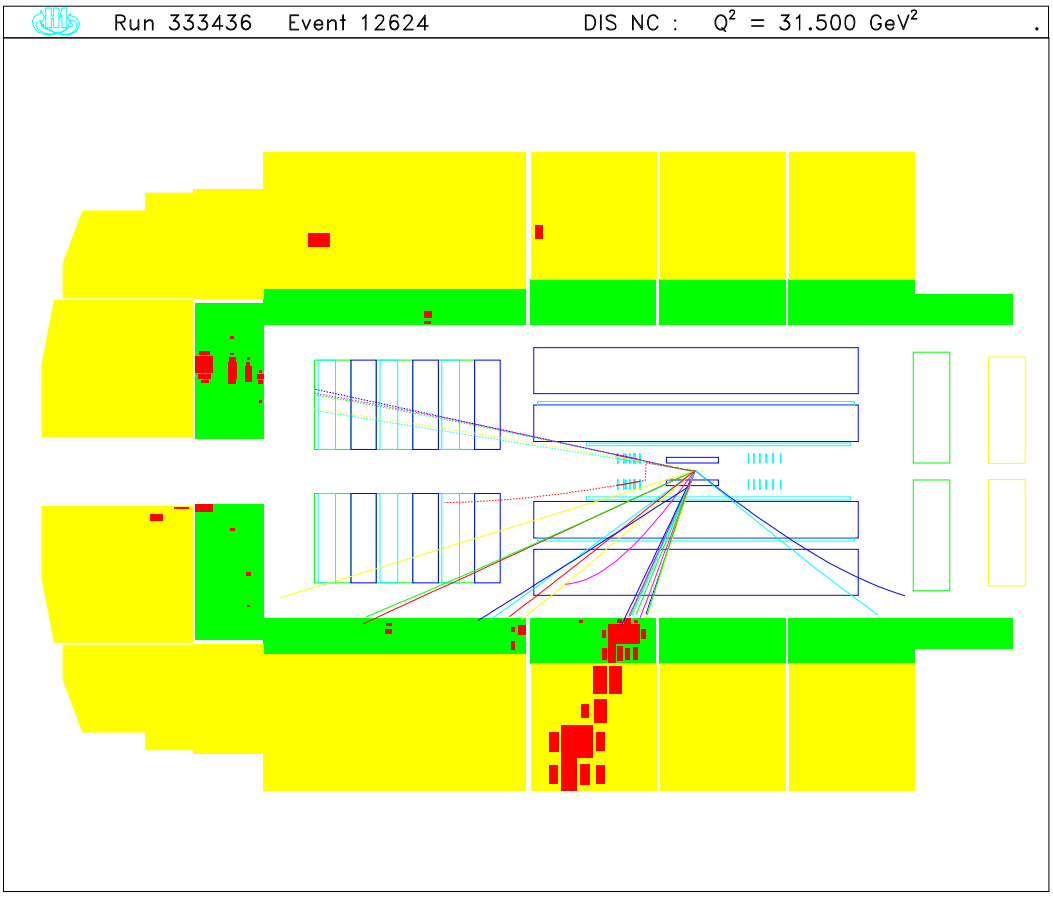

Figure 2: The highest Q^2 event recorded by the H1 detector in the 2002 run period.

HERA passed an important milestone in late December, when a luminosity similar to the best achieved before the upgrade was reached. The product of the beam currents was a factor of four lower than that previously necessary to achieve this luminosity. The new machine's capabilities have thus been demonstrated and the solution of the background problems, plus the development of procedures to ensure stable and reliable running, will allow the collider experiments to collect the $1\,\mathrm{fb}^{-1}$ of high energy data and the data with lower proton beam energies foreseen for the HERA II physics programme.

2 Current background situation

The development of the backgrounds in the H1 detector is illustrated in figure 3, which shows the CJC currents as a function of positron current, corrected to a proton current of 30 mA, for various running periods. The situation has improved considerably during the last few months,

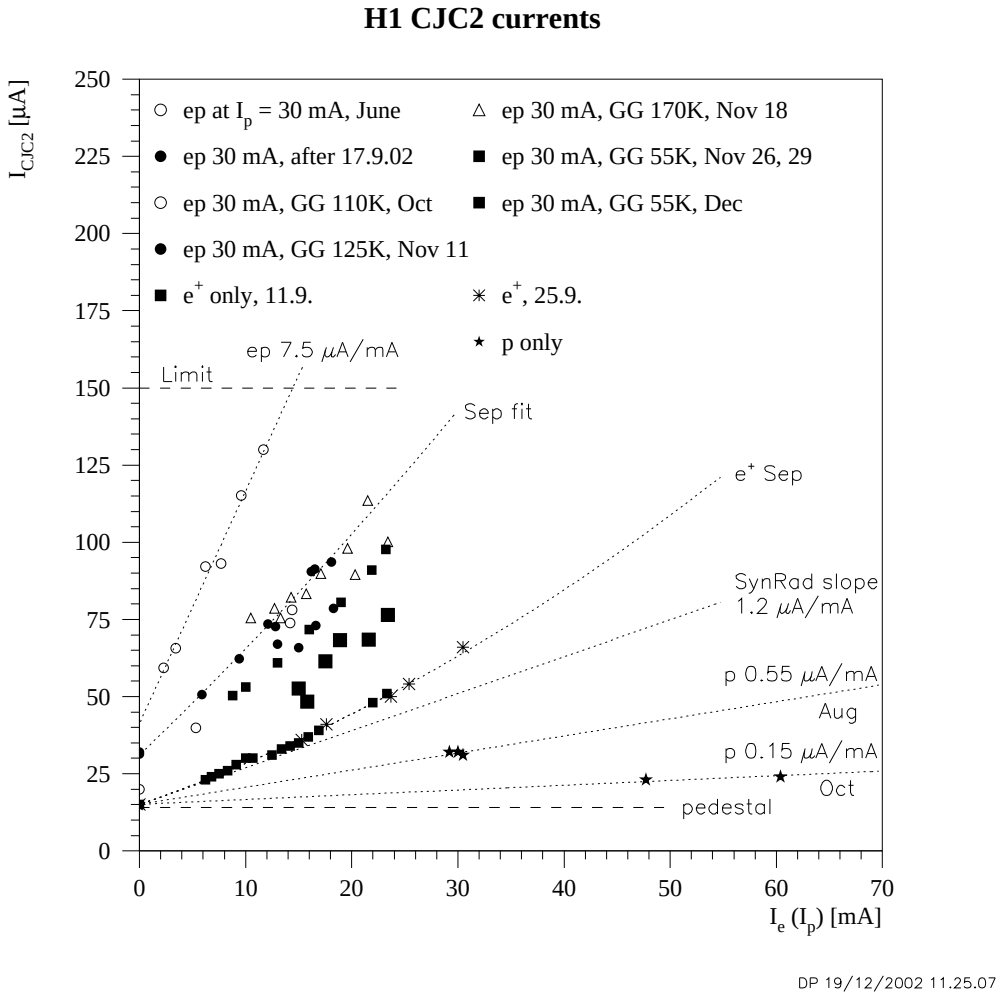

Figure 3: The currents in CJC2 as a function of the positron beam current for various running periods. The CJC2 currents are corrected to a proton current of 30 mA, as described in [1].

in particular at the beginning of December 2002. Extrapolation of the results from the best runs in December to the limiting CJC currents of $150 \ldots 200\,\mu$A shows that backgrounds in H1 decreased to within a factor of about two of what is necessary for safe operation at the design positron and proton beam currents of 58 mA and 135 mA, respectively. The situation deteriorated somewhat towards the end of December meaning that an improvement of a factor of about three is required over the conditions pertaining at the end of the 2002 running period.

As described in [1], at design HERA currents the majority of the background in the H1 detector results from the re-scattering in the material around the beam line of particles produced in primary proton beam-gas interactions. The rate of these primary interactions is dependent on the pressure in the beam pipe, which is influenced by the current and energy of the positron beam. It is thought that synchrotron radiation and Higher Order Mode (HOM) heating cause

desorption of gasses deposited on the inner surfaces of the vacuum chambers. Much of this report is concerned with investigations of this aspect of the background problem.

2.1 Sensitivity of H1 to proton-induced background

Significant changes were made to both the HERA machine and the H1 detector during the lumi-

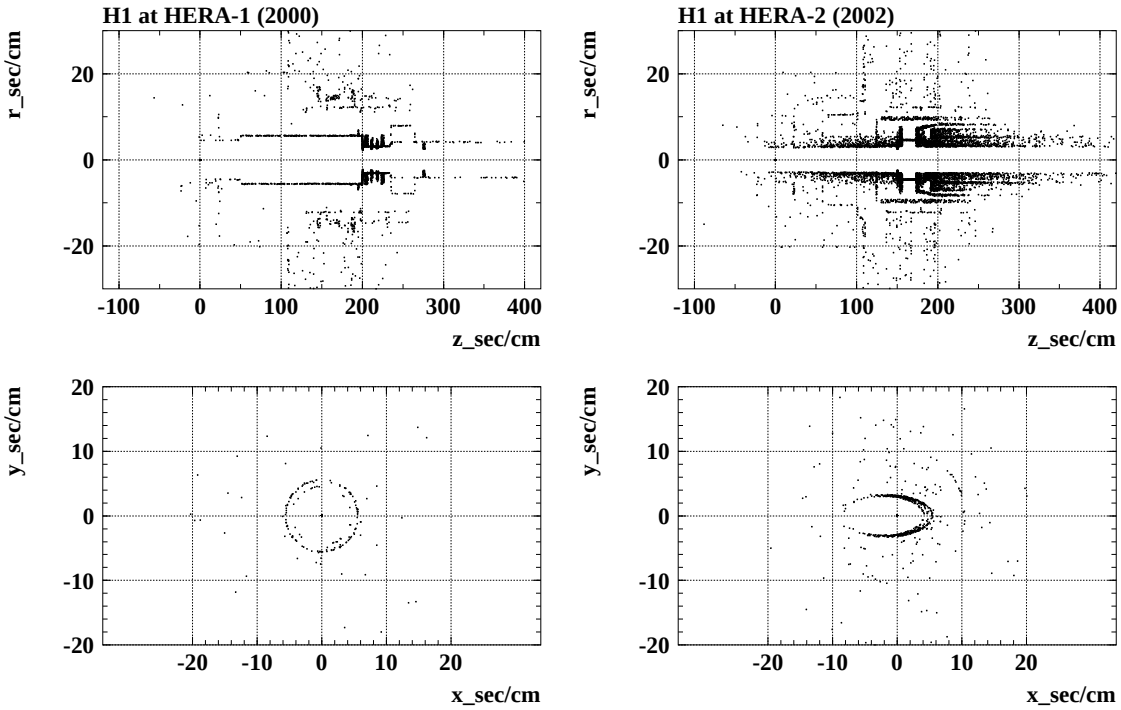

Figure 4: The positions of secondary vertices in simulated proton beam-gas events in the H1 detector as it was in the year 2000 (left) and as it now is (right) in both the r-z (top) and x-y planes (bottom). The latter plot was made with the requirement that the primary z vertex be within ± 60 cm of the IP.

nosity upgrade. One factor contributing to the larger backgrounds observed since the upgrade may be an increased sensitivity of the detector arising from the tighter apertures, additional magnets, collimators *etc.* within and surrounding H1. Detailed Monte Carlo simulations of the H1 detector in its pre- and post-upgrade states were made to investigate this possibility. The tighter apertures in and around H1 following the upgrade are clearly visible in figure 4, which shows the positions of secondary vertices in proton beam-gas events with detector configurations as in the years 2000 and 2002. The consequences of this for the backgrounds in H1 are illustrated in figures 5 and 6. The former shows the position of the z vertex of primary proton beam-gas interactions that cause backgrounds in various parts of the H1 detector. The additional material around the beam pipe is observed to have a screening effect. For example, following the upgrade, the H1 CJC is sensitive to primary interactions out to $z \gtrsim -20$ m, while prior to the upgrade this sensitivity extended further from the detector. However, as shown in figure 6, the additional material close to the beam line in 2002 causes the charged multiplicity produced in the secondary interactions following the above primary scatters to be higher than it was in

2000. Thus, although H1 is now sensitive to proton-induced background caused by primary interactions in a smaller z range than used to be the case, those primary interactions that do occur cause larger backgrounds. The net effect for the CJC is that, for a comparable vacuum situation, the chamber currents produced post-upgrade are a factor of about 1.5 higher than they were prior to the upgrade for given beam currents.

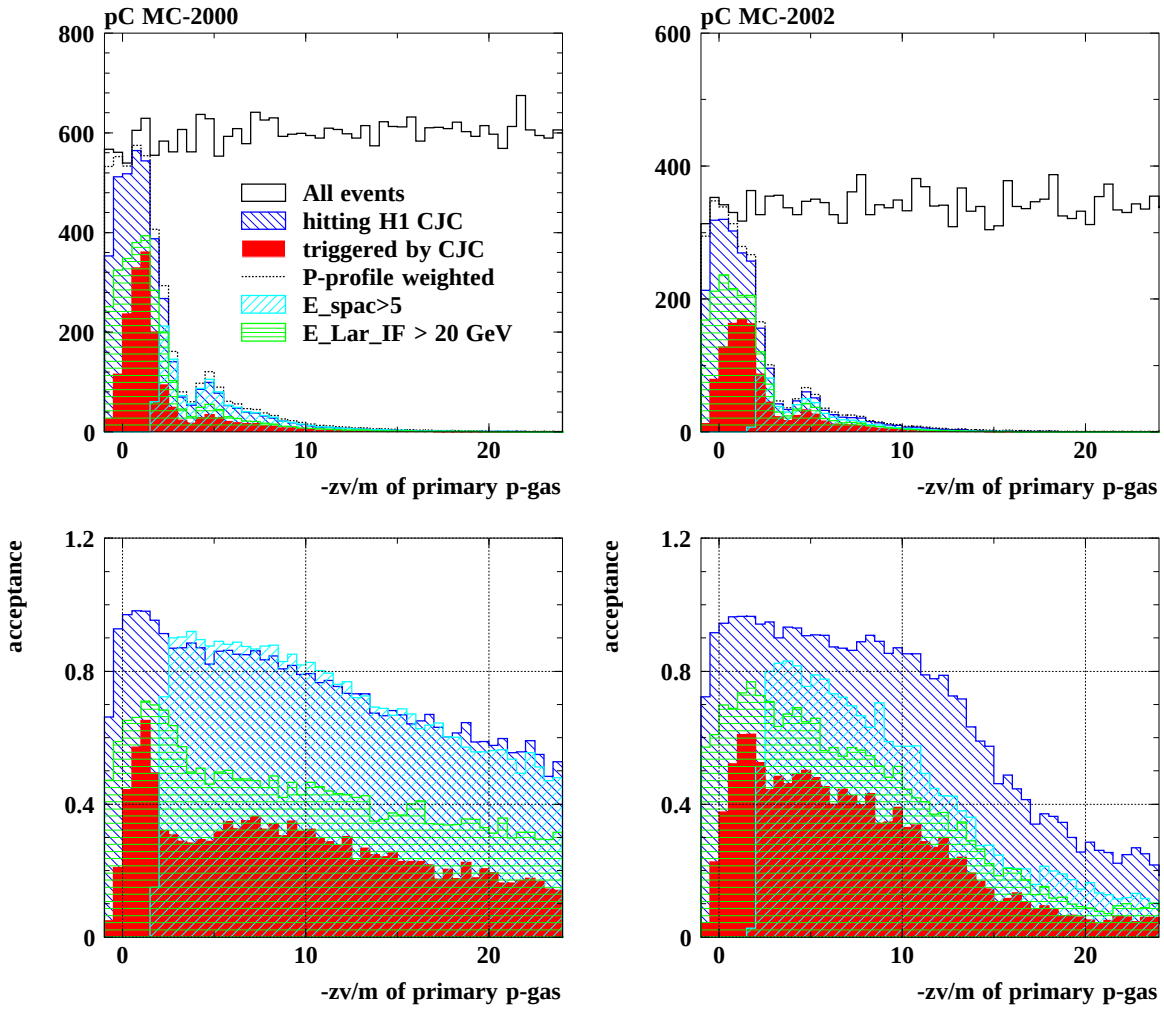

Figure 5: Upper plots show simulated distributions of the z vertex of primary proton beam-gas interactions assuming both a flat and a realistic pressure profile as well as z vertex distributions for primary interactions which directly or via re-scattering cause background signals in various of the H1 detectors for the years 2000 (left) and 2002 (right), together with the resulting acceptances (lower plots) for the two periods.

2.2 Composition of residual gas within H1 interaction region

The pressure in the HERA beam line is measured by monitoring the currents drawn in getter pumps (GPs) distributed around the ring, while the composition of the residual gas can be measured by using residual gas analysers (RGAs). These can be connected to the vacuum chambers via ports left and right of the experiments. An overview of the vacuum pumps and

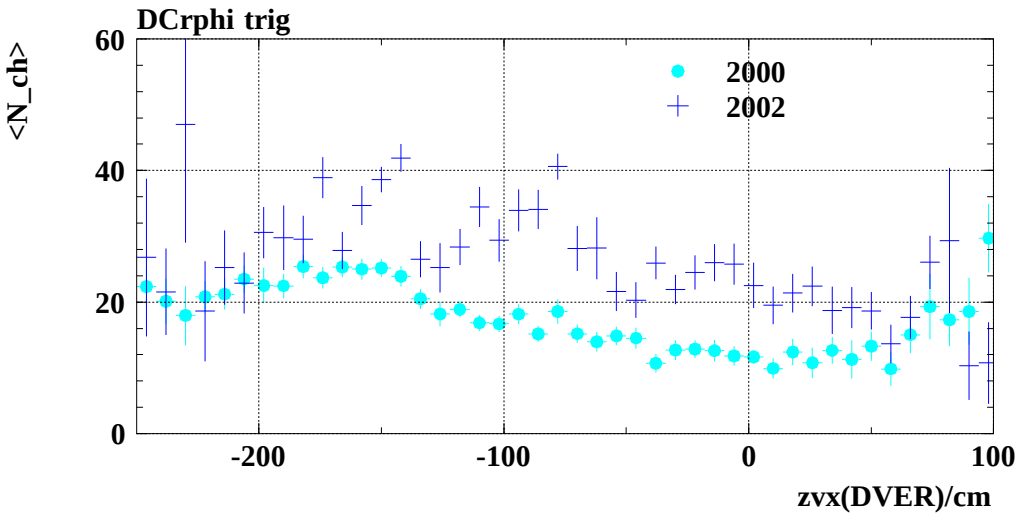

Figure 6: The simulated mean charged multiplicity seen in the CJC as a function of the measured z vertex position in the years 2000 and 2002 for track triggered events.

available ports is given in figure 7. Unfortunately, the ports closest to H1 are some $26\,\mathrm{m}$ from the interaction point (IP) and the gasses pass over $20\,\mathrm{m}$ of non-evaporable getter (NEG) pumps incorporated in the HERA vacuum chambers and several getter and titanium sublimation pumps (TSPs) between the IP and the RGA. It is thus possible that the composition measured in the RGA differs significantly from that at the IP. Further, the RGA cannot be operated while there are beams in HERA, so changes in the residual gas composition due to the effects of the beams cannot be detected.

In order to overcome the above problems in the short term, measurements of the residual gas composition within the H1 experiment were performed by studying the charged multiplicity of proton beam-gas interactions close to the H1 interaction point and comparing the results with Monte Carlo simulations, as described in [1]. In the longer term, a residual gas analyser will be installed close to the H1 IP. The multiplicity studies indicate that a significant proportion of the p-gas interactions involve atoms or molecules which are significantly heavier than hydrogen. As is shown in figure 8, the observed multiplicities are larger than those measured in proton-proton interactions and match better the expectations for proton-carbon or proton-oxygen collisions.

The chemical composition of the residual gas in accelerator vacuum systems is known to change as a function of beam dose, as is described in [2]. Typically, early in the life of a vacuum chamber, the residual gas is composed of H_2, CO_2, CO, CH_4 and H_2O. Following exposure to the beams, the residual gas is composed primarily of H_2 and CO. As is clear from figure 8, the multiplicity observed within H1 is consistent with the residual gas being composed largely of carbon monoxide, water and/or other species of similar molecular weight, *c.f.* figure 27.

The cross section for the interaction of protons with nuclei rises with the mass of the nuclei, so one possible cause of the increased background levels in 2002 as compared to previous years is an increase of the average mass of the nuclei in the residual gas. This was investigated by performing the same charged multiplicity study using data taken in $1997 \ldots 2000$ and Monte Carlo simulations of the HERA beam line and the H1 detector in the appropriate configurations. The results, shown in figure 9, suggest that the composition of the residual gas has not changed significantly since 2000.

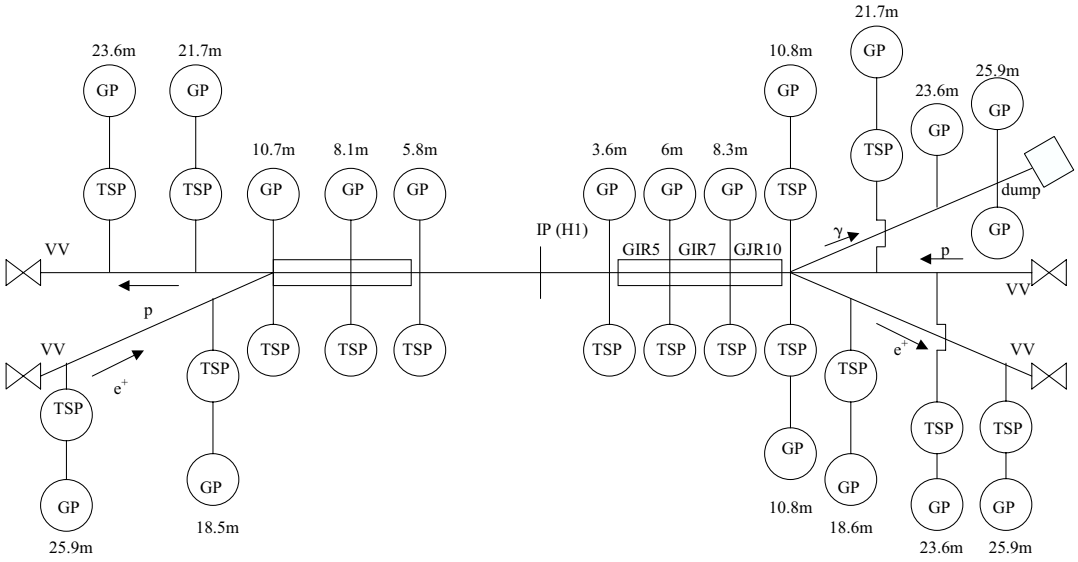

Figure 7: The location of the titanium sublimation pumps (TSPs), getter pumps (GPs) and the positions at which mass spectrometers can be connected near the H1 interaction region (VV). Not shown are the non-evaporative getter pumps which are incorporated in the HERA vacuum chambers.

2.3 Pressure of the residual gas within the H1 interaction region

2.3.1 Pressure measurement using Bethe-Heitler events

Having demonstrated that the composition of the residual gas is reasonably constant, it is possible to investigate the pressure of the gas close to the interaction region as a function of time by studying the rate of Bethe-Heitler events in which the scattering occurs off a gas nucleus. The fraction of the rate of Bethe-Heitler events measured in the luminosity system due to positron beam-gas scattering is given by

$$f^{e-gas} = \frac{\sigma^{eZ}_{BH}(E) \cdot I_e/q_e \cdot N_A \cdot P \cdot L_z}{\sigma^{ep}_{BH}(E) \cdot \mathcal{L}},$$

where $\sigma^{eZ}_{BH}(E)$ and $\sigma^{ep}_{BH}(E)$ are the cross-sections for Bethe-Heitler scattering off the nucleus and proton, respectively, as a function of the positron energy E. The positron beam current is represented by I_e and q_e is the positron charge, N_A is the Avogadro number, P is the residual gas pressure and L the length over which the luminosity system is able to detect Bethe-Heitler events. The higher the residual gas pressure, the larger will be f^{e-gas}. Experimentally, this fraction can be determined by comparing the rates of Bethe-Heitler events for colliding and positron pilot bunches. Results for f^{e-gas}_{1995} are shown in figure 10. The year 1995 is analogous to 2002 in that running started following a shutdown in which the beam pipe was vented. The initially poor vacuum conditions are seen to improve over a period of roughly 200 days. The

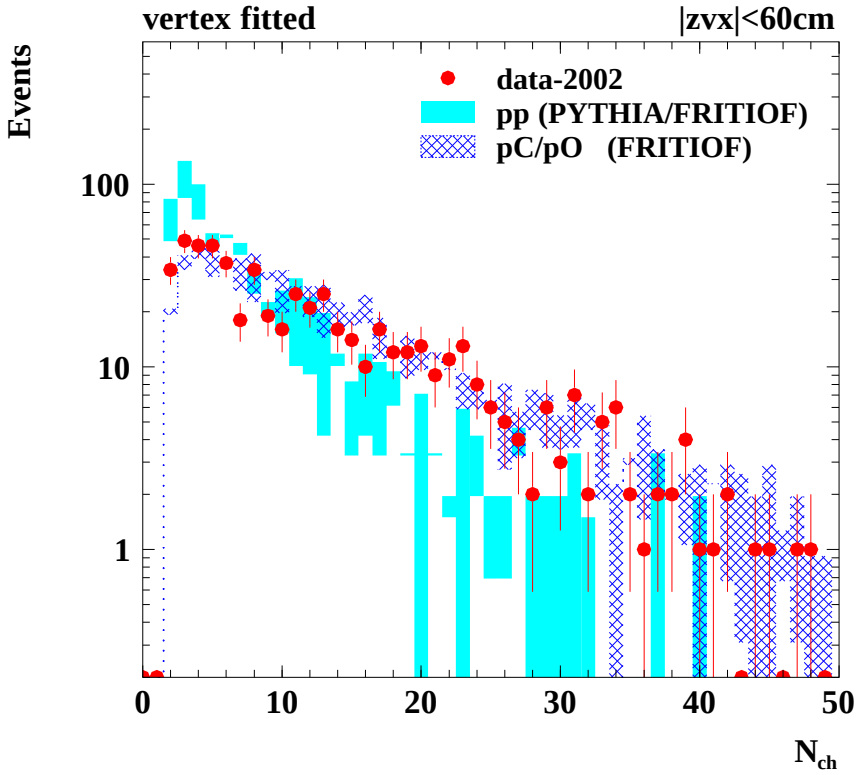

Figure 8: The charged multiplicity of proton beam-gas events observed in 2002 with primary vertex close to the H1 interaction point compared with the expectations for proton-proton interactions (the band indicates the uncertainties arising from using two alternative Monte Carlos) and the interactions of protons with carbon and oxygen (the band indicates the range expected for these two nuclei).

vacuum then deteriorates following a leak and improves until only $\sim 2\%$ of Bethe-Heitler events are due to beam gas. In subsequent years, the fraction of Bethe-Heitler events due to beam gas scattering is seen to decrease to a minimum of about $2 \ldots 3\%$, a value that is maintained throughout 2000. This appears to represent the best achievable vacuum with the HERA I beam pipe and vacuum pump system. The resulting good experimental conditions helped to ensure that the year 2000 was the most successful in HERA's history to date. It is used as the base line in the following comparisons.

Given that the gas composition in, for example, the years 2000 and 2002 is very similar, as shown above, the expression for the double ratio of the fractions of the Bethe-Heitler rates in the two years is particularly simple, namely

$$R = \frac{f_{2002}^{e-gas}}{f_{2000}^{e-gas}} = \frac{P_{2002}}{P_{2000}} \cdot \frac{L_{2002}}{L_{2000}} \cdot \frac{I_e^{2002}}{I_e^{2000}} \cdot \frac{\mathcal{L}_{2000}}{\mathcal{L}_{2002}}.$$

As the ratio $L_{2000}/L_{2002} = 12\,\mathrm{m}/4\,\mathrm{m} = 3$, the result

$$\frac{P_{2002}}{P_{2000}} = 3R \cdot \frac{I_e^{2000}}{I_e^{2002}} \cdot \frac{\mathcal{L}_{2002}}{\mathcal{L}_{2000}}$$

is obtained. Results for the ratio P_{2002}/P_{2000} are shown in figure 11. As expected, the pressure

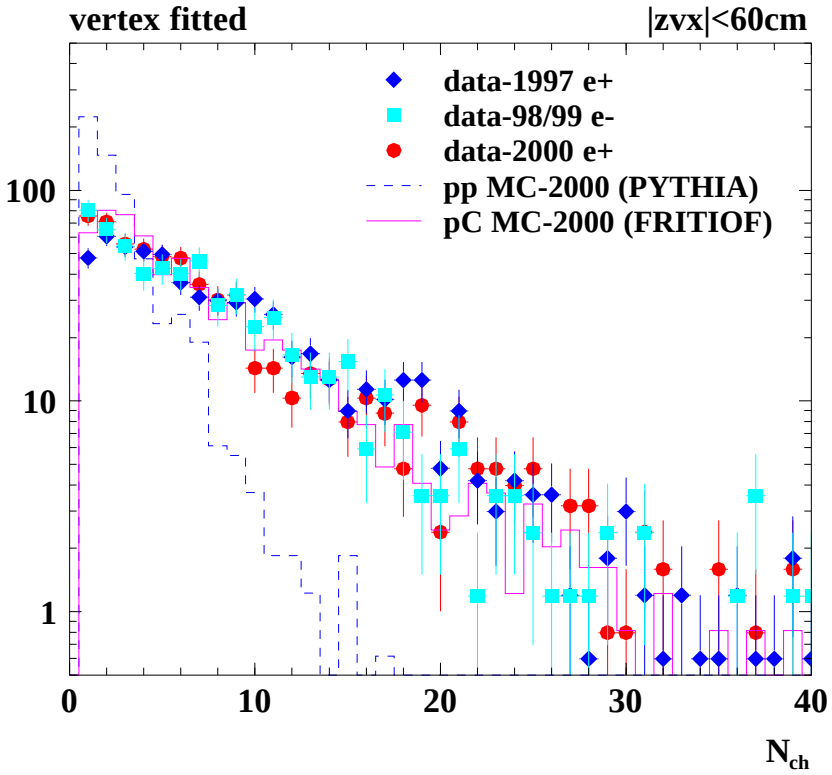

Figure 9: The charged multiplicity of proton beam-gas events observed in $1997 \ldots 2000$ with primary vertex close to the H1 interaction point compared with the expectations for the interaction of protons with various nuclei.

is seen to depend on the positron current; with small currents the conditions are better than with large currents. Concentrating on the measurements made with $I_e > 10\,\mathrm{mA}$, the initially poor vacuum conditions are seen to gradually improve, again over a period of roughly 200 days, but then the behaviour becomes more complicated, before a further drop is seen to pressures that approach those observed in 2000. The last few runs in 2002 saw a rise in pressure to values about 3 to 4 times those observed in 2000. This behaviour will be discussed in more detail in the following. Note that the average positron current in 2000 was $25\,\mathrm{mA}$.

2.3.2 Pressure measurement using proton beam-gas events

A second comparison of the pressure in the H1 vacuum chamber in 2002 with that in 2000 can be obtained from the ratio of the rates of proton beam gas events in the two running periods. The constancy of the composition of the residual gas ensures that the rates are proportional to the pressure in the H1 vacuum chamber and the proton beam current. Figure 12 shows the distribution in x and y of vertices reconstructed within $\pm 60\,\mathrm{cm}$ of the nominal interaction point in z for randomly triggered events taken throughout the year 2000 and for a random trigger run taken on November 12^{th} 2002. Beam gas events are selected using the requirement that the event vertex be within a radial distance of $1\,\mathrm{cm}$ of the nominal beam line in both cases. For the year 2000, some 599 beam gas events were reconstructed out of a total of 1.745×10^6 random events. From the random trigger run taken in November 2002, 141 events pass the proton beam-gas selection out of a total of 0.51×10^6. Taking into account the fact that the average proton

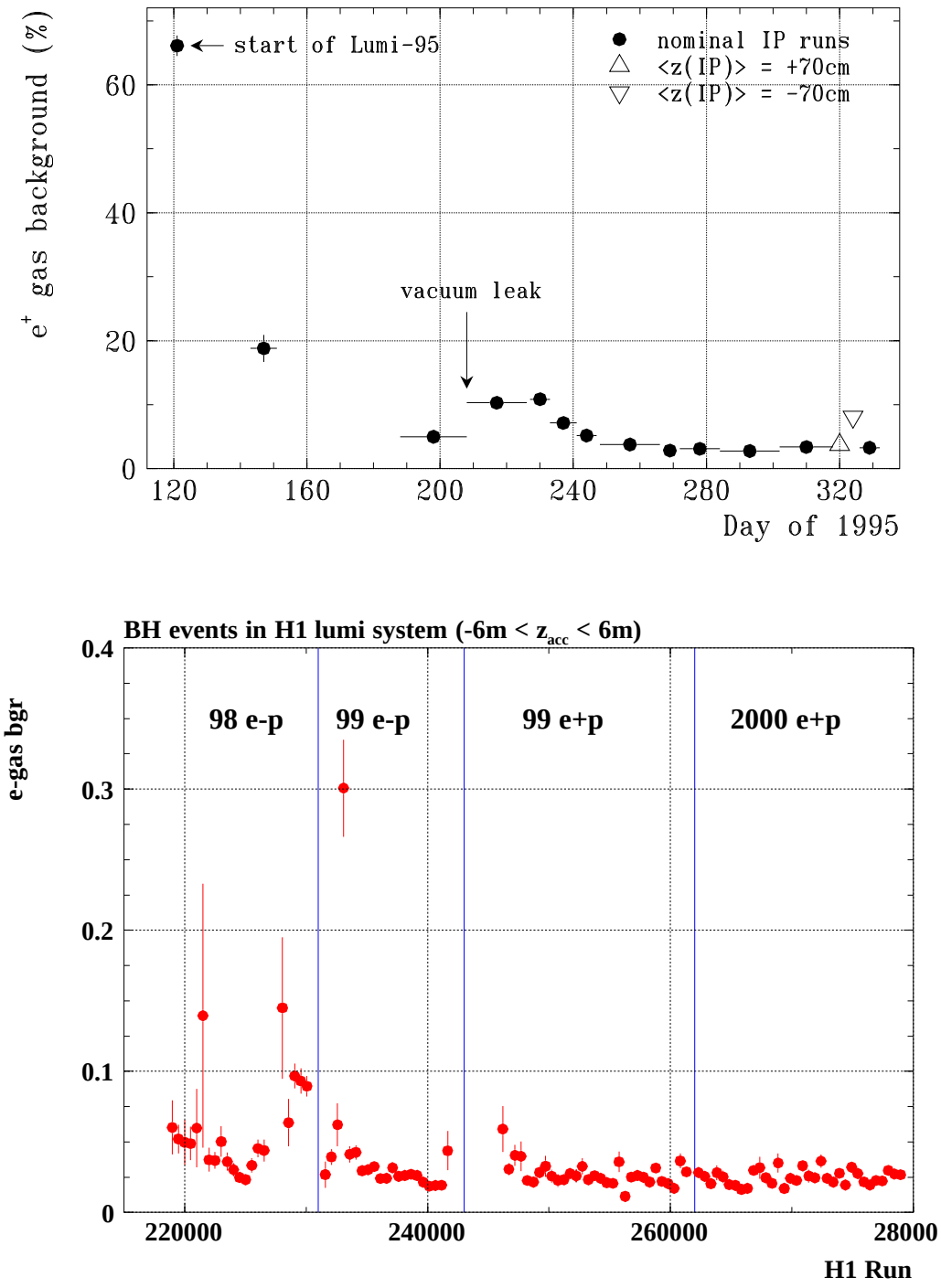

Figure 10: The proportion of Bethe-Heitler events induced by positron beam-gas scattering in the year 1995 (upper plot) together with the same proportion for HERA runs in 1998 . . . 2000 (lower plot).

beam current in 2000 was 86.8 mA, while it was only 17.2 mA for the November run, a pressure ratio of $\simeq 4.1$ between November 2002 and the average of 2000 is obtained, consistent with the value extracted in the e-gas analysis presented in section 2.3.1 for this period. Note that the average positron current of 25.1 mA in 2000 was significantly higher than that of 17.1 mA recorded during the November run.

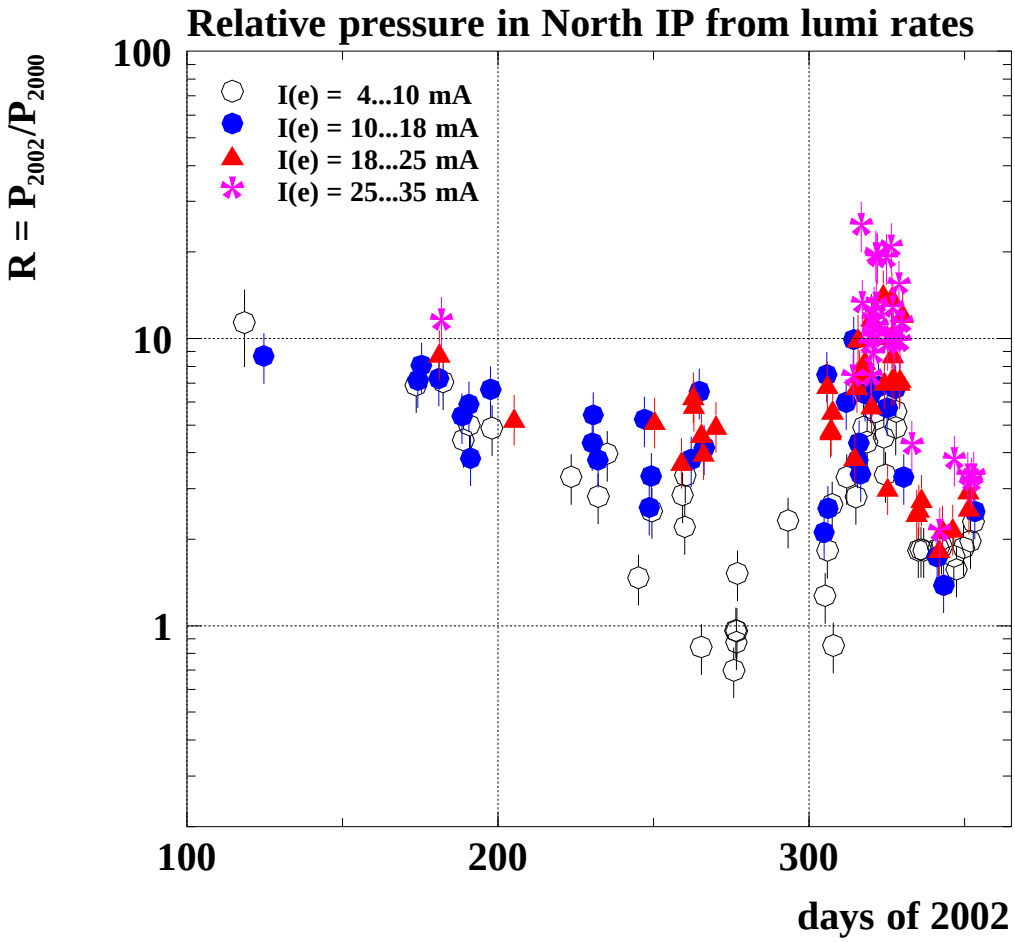

Figure 11: The ratio of the pressure in the H1 interaction region in the year 2002 to that in the year 2000, measured using the rate of Bethe-Heitler events induced by beam gas. The high pressures around day 320 are associated with the running of the GO and GG magnet shields at relatively high temperature, see text.

2.4 Absolute pressure of the residual gas within the H1 interaction region

The method described in section 2.3.1 can be extended to give the absolute pressure in the H1 interaction region if the composition of the residual gas is known. Assuming the mean atomic number of the atoms composing the gas is $\langle Z \rangle = 5$, as obtained in [1] and supported by the results illustrated in figure 8, the ratio of the cross sections for Bethe-Heitler scattering on protons and the residual gas nuclei is $\sigma^{eZ}_{BH}(E)/\sigma^{ep}_{BH}(E) = 8.0 \pm 0.3$, where the uncertainty arises by allowing for varying levels of screening of the nuclear charge. The pressures shown in figure 13 as a function of positron beam current are then obtained for the years 1998 to 2000. These can be reasonably represented by linear functions of the positron current, as illustrated in the figure, as would be expected if the dynamic pressure increase is caused by outgassing induced by synchrotron radiation. There is perhaps some evidence of the need for a steeper increase of pressure with current at the highest positron currents in the year 2000.

Extending this analysis to the year 2002 and considering only data taken until the end of November, *i.e.* before the improvement in background conditions at the end of the 2002 run-

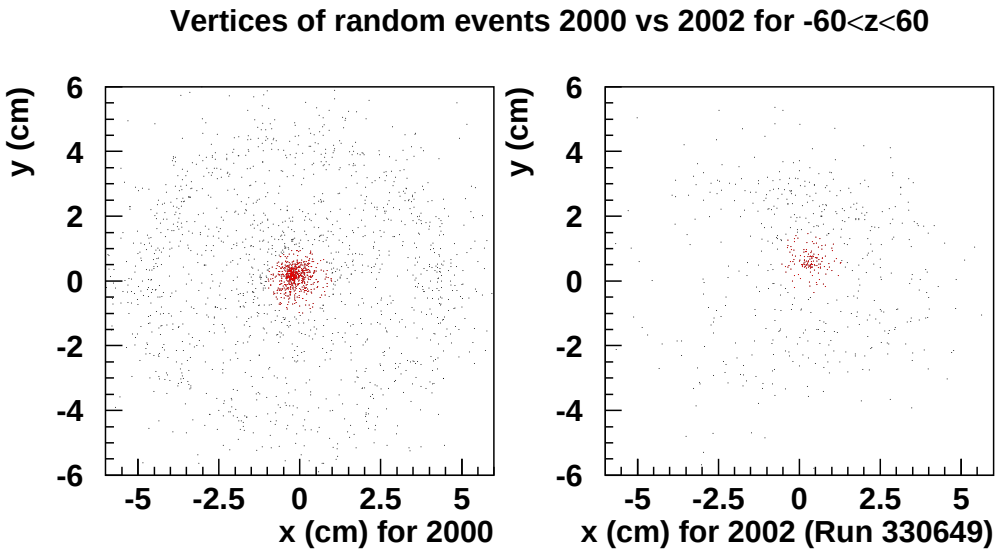

Figure 12: Vertex distributions of all randomly triggered events taken in the year 2000 (left) and for a random trigger run taken on 12^{th} November 2002 (right). The different shapes of the beam pipes can be seen. Beam gas events are selected by a radial cut around the nominal beam spot.

ning period, leads to the results shown in figure 14, upon which are superimposed the functions describing the pressure in the years 1998 to 2000. The pressure increase with positron current during the period with particularly poor background conditions in 2002 is much more dramatic than in previous years, demonstrating that a major change between the situations before and after the upgrade is the degree to which the positron beam affects the vacuum. There is some evidence of a non-linear component in the relationship between the positron current and pressure, particularly at the highest positron beam currents. This may indicate that mechanisms other than desorption induced by synchrotron radiation are involved in the outgassing which causes the deterioration of the vacuum in 2002. This possibility, which applies particularly at injection energies, will be addressed later in this report.

2.5 Development of the absolute pressure with time in 2002

The spread of the points describing the relationship of the pressure in the H1 interaction region with the positron beam current in figure 14 is partly due to the change in that relationship through the 2002 running period. This is shown explicitly in figure 15, in which the pressure, determined using the method described in section 2.4, is shown as a function of time for four ranges of positron beam current. The figure also illustrates the pressures typical for these positron currents in the year 2000. The pressure is seen to fall by roughly an order of magnitude over a period of about 250 days and, at the higher positron currents, to lie about a factor of three above the top of the range observed in the year 2000 by the end of 2002. The decrease with time is, however, not monotonic. At around day 300 of the year 2002, the pressure is observed to increase for all positron currents for a period of roughly 25 days. During this period experiments were conducted in which the HERA machine was operated with the beam pipe within the GO and GG magnets at temperatures well above the nominal $55\,\text{K}$. These experiments are described in section 3.2.

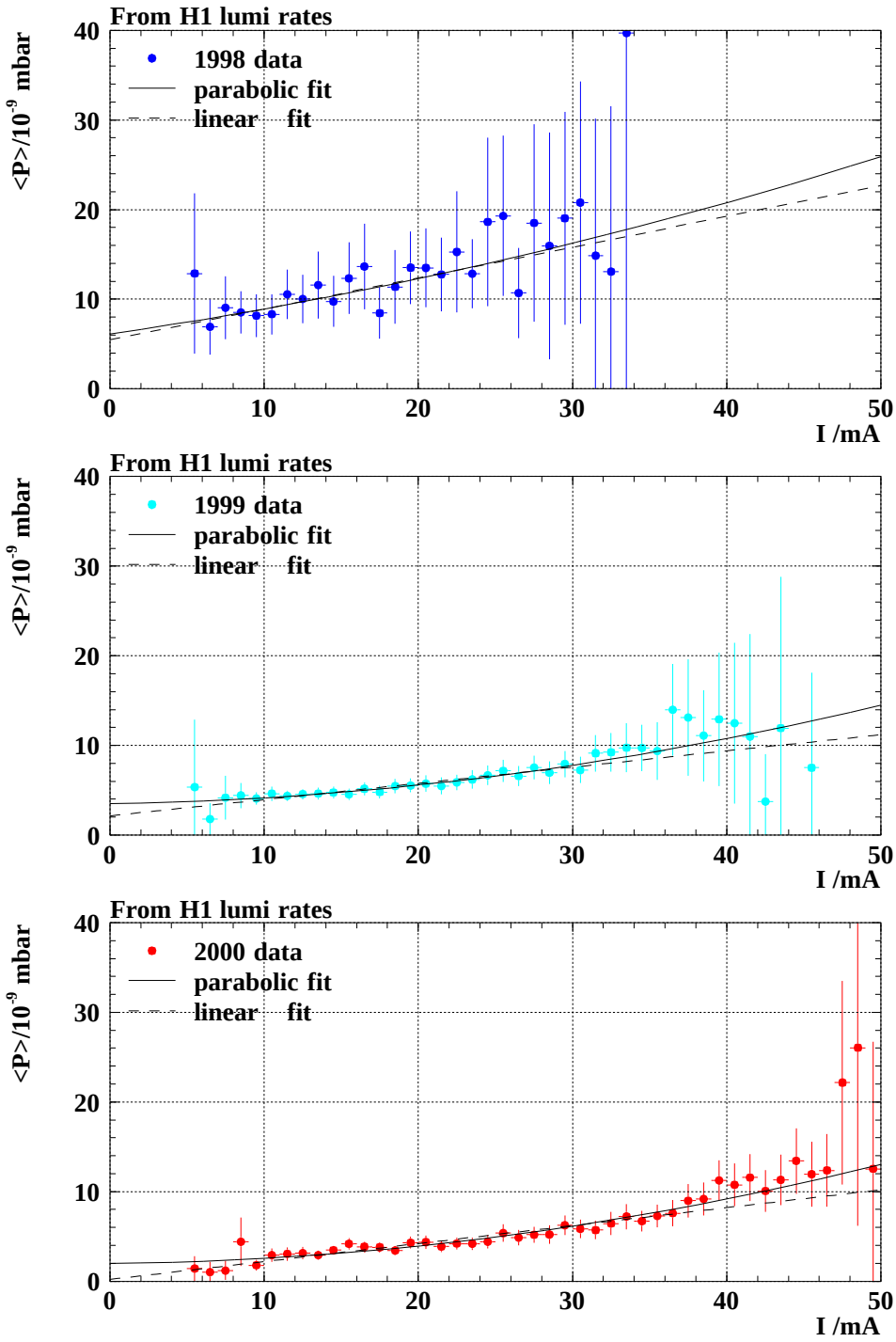

Figure 13: The absolute pressure in the H1 interaction region in the years 1998 to 2000 shown as a function of positron beam current.

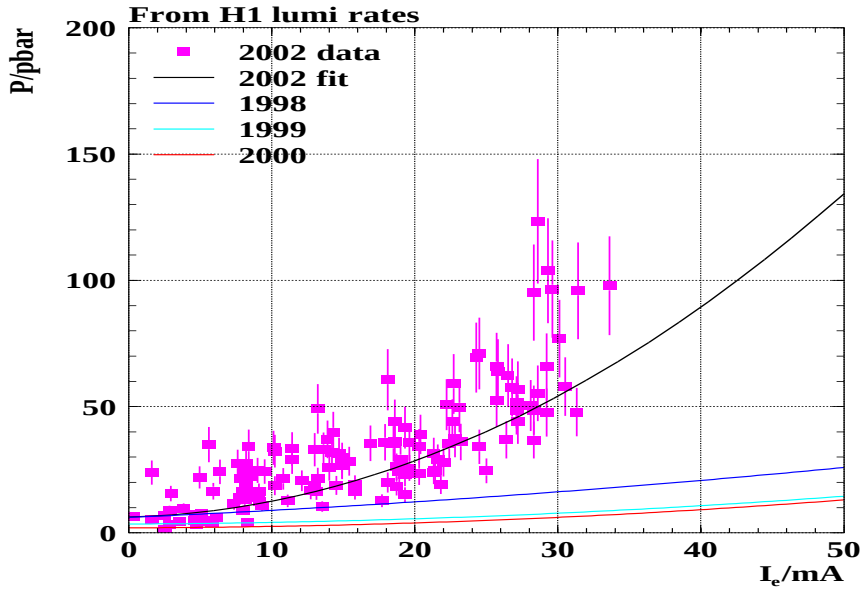

Figure 14: The absolute pressure in the H1 interaction region in a period in 2002 in which the background conditions were poor (data points) shown as a function of positron beam current and compared with curves describing the pressure in the years 1998 to 2000, derived from the results shown in figure 13.

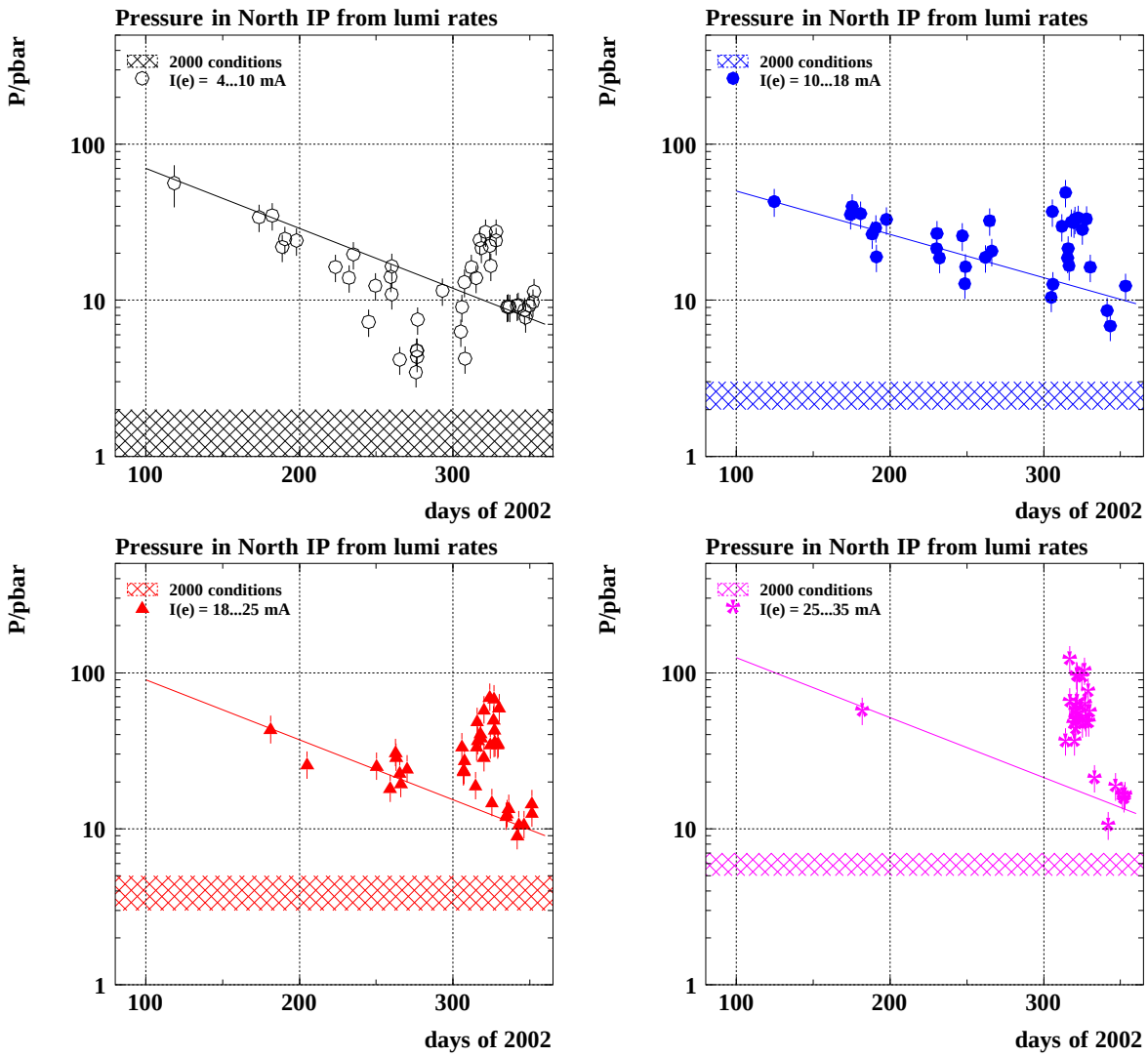

Figure 15: The absolute pressure in the H1 interaction region in the year 2002, shown for various ranges of positron beam current with a line illustrating the approximate pressure drop with time, when the excursion to higher pressures in the period between about 300 and 325 days is ignored. The shaded bands indicate the pressure range observed in the year 2000 for the relevant positron currents.

2.6 Investigation of backgrounds in the H1 central detectors

2.6.1 Currents in the Central Jet Chamber

The dependence on the beam conditions of the currents measured in the H1 drift chambers, and how that dependence has changed with time, has proven to be a sensitive means of disentangling the various contributions to the backgrounds in H1. The same applies to the rates measured in the radiation monitor. The currents drawn by the inner and outer central drift chambers, CJC1 and CJC2 respectively, receive contributions from synchrotron radiation ($\propto I_e$), positron beam-gas interactions ($\propto I_e$ and P_L, the pressure in the vacuum chambers to the left of and within H1) and proton beam-gas interactions ($\propto I_p$ and P_R, the pressure in the vacuum chambers to the right of and within H1), *i.e.*

$$I_{\mathrm{CJC}} = I_0 + \alpha_{SR} I_e + \alpha_e I_e \langle P_L \rangle + \alpha_p I_p \langle P_R \rangle, \tag{1}$$

where I_0 is a small chamber pedestal current. Assuming that the average pressure depends linearly on the positron beam current and is given by $\langle P_L \rangle = P_0^L + \gamma_L I_e$ and $\langle P_R \rangle = P_0^R + \gamma_R I_e$, with P_0^L and P_0^R representing the base pressure to the left and right of H1, the following parameterisation is obtained

$$I_{\mathrm{CJC}} = a_0 + a_1 I_e + a_2 I_e^2 + a_3 I_p + a_4 I_e I_p. \tag{2}$$

Here, $a_1 = \alpha_{\mathrm{SR}} + \alpha_e P_0^L$ is a measure of the contribution from synchrotron radiation and from positron beam-gas at the base pressure, $a_2 = \alpha_e \gamma_L$ of the dynamic e-gas contribution, $a_3 = \alpha_p P_0^R$ of the proton beam-gas contribution at the base pressure and $a_4 = \alpha_p \gamma_R$ is a measure of the contribution arising from the interplay of both beams.

In order to study the development of the various contributions to the background, the variation of the coefficients a_i during 2002 was investigated for CJC2. The pedestal current was small and very stable at about $15\,\mu$A. The coefficients a_1 and a_2 were determined during positron only runs which exhibit a quadratic dependence of the CJC current on I_e and were observed to be relatively stable. The coefficients a_3 and a_4 were determined by fitting the I_e and I_p dependence of the CJC2 currents in long runs. Figures 16 and 17 show the time development of these coefficients. The coefficient a_3 is shown together with the base pressure, as measured by the pump at NR 3.6 m, and exhibits no significant time dependence. The coefficient a_4 decreases with time. In figure 17 it is shown with the dynamic pressure ($\Delta p / \Delta I_e$) development at four pump stations to the right of the IP, which show a comparable decrease with time. A similar study of the pressures to the left of the IP as a function of I_e reveals little change in the dynamic pressure as a function of time.

The overall development of the CJC2 current with time is shown in figure 18. One observes that the chamber current expected at the HERA design beam currents of $I_e = 58\,$mA and $I_p = 135\,$mA decreased from about 1000 μA, or even higher values, to a few 100 μA over a period of about 4 months. At the end of 2002 the CJC currents at design beam currents were within a factor of about 3 of the limits considered tolerable if the chamber is to survive a further five years of HERA operation.

An independent analysis gives rise to the coefficients shown in table 1. Unfortunately, a positron only run scheduled for the end of December was not taken, so the a_1 and a_2 values in

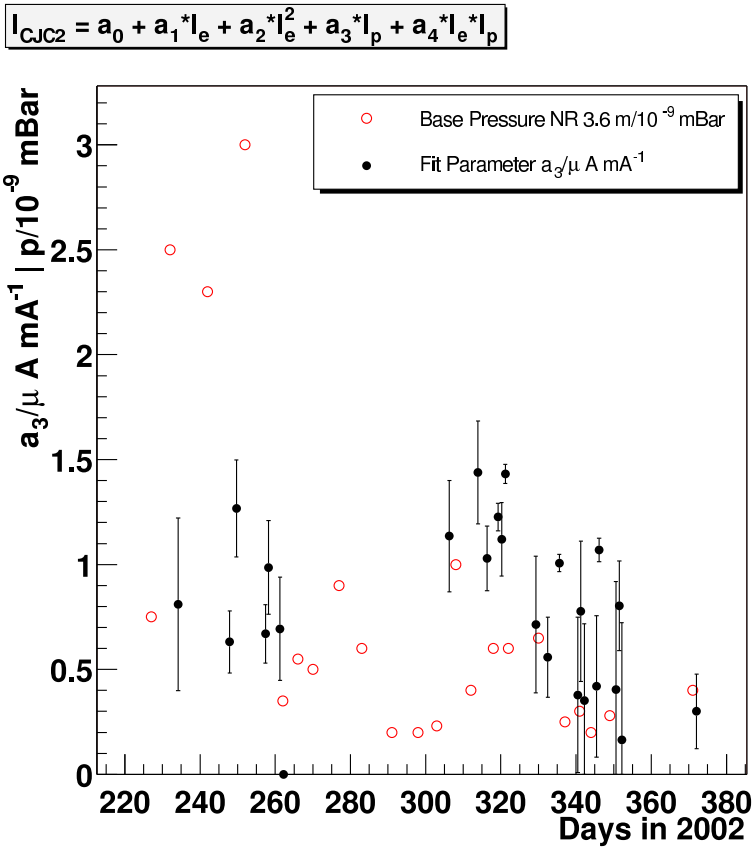

Figure 16: Time dependence of the coefficient a_3 (closed circles) characterising the relative amount of the contribution $\propto I_p$ to the current drawn by the outer central H1 drift chamber, CJC2. The open circles represent the static pressure at NR 3.6 m in units of 10^{-9} mbar for comparison.

the table for December are taken to be the best attained up to that point. This is supported by measurements made in January 2003 which show a behaviour compatible with that in September 2002. The improvement in the background situation in December is then found to be due primarily to the reduction in the coefficient a_4, *i.e.* again due to the significantly reduced effects of the positron beam on the vacuum. Further long runs in which there is a large range of beam currents with otherwise stable conditions will allow this hypothesis to be tested more stringently.

Coefficient	August	September	November	December
a_0 (μA)	15.0	15.0	15.0	15.0
a_1 (μA/mA)	1.5	1.2	1.2	*1.2*
a_2 (μA/mA^2)	0.017	0.014	0.052	*0.014*
a_3 (μA/mA)	0.72	0.54		0.23
a_4 (μA/mA^2)	0.11	0.070		0.025

Table 1: Coefficients necessary to describe the CJC2 currents as a function of the beam currents using equation 2. Entries in italics are assumed values only.

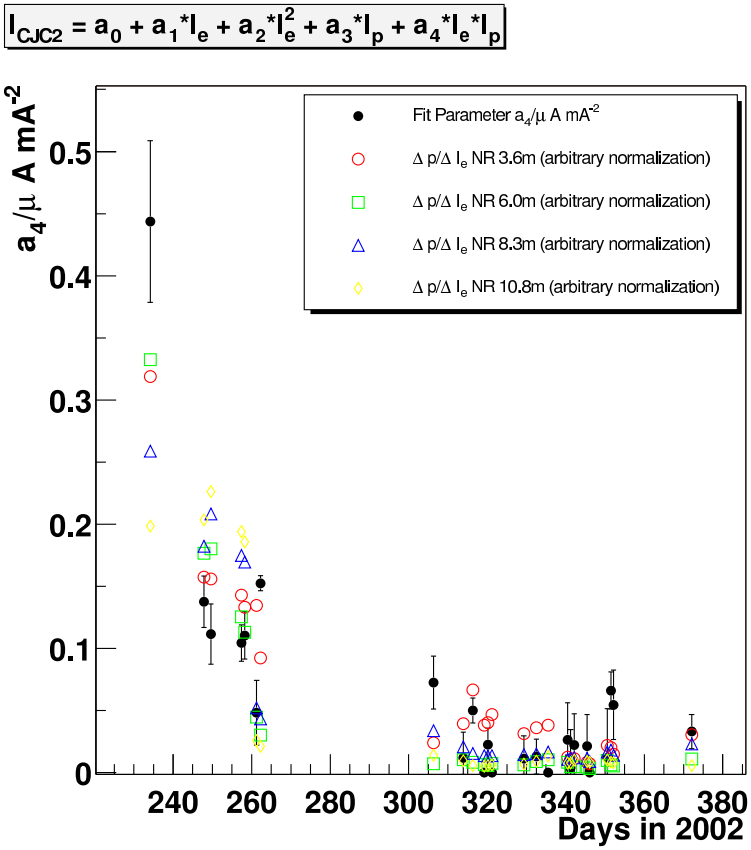

Figure 17: Time dependence of the coefficient a_4 (closed circles) characterising the relative amount of the dynamic contribution $\propto I_p \cdot I_e$ to the current drawn by the outer central H1 drift chamber, CJC2. The open symbols represent the dynamic pressure at four positions right of the interaction point, *i.e.* the change of pressure per unit change in positron current.

2.6.2 Rates in the Radiation Monitor

The rate measured in the silicon pad detector, which serves as a radiation monitor, is highly correlated with the currents observed in the CJC, as can be seen in figure 22. The correlation is approximately linear for all conditions, the pad detector rate approaching zero for a CJC2 current of $15\,\mu$A, the pedestal value. A limit of about 50 kHz for 30 minutes, or 250 kHz for 5 minutes, was determined as the tolerable dose, which corresponds closely to the $150\,\mu$A limit set by the drift chamber.

The radiation monitor was on almost continuously, allowing the monitoring and feedback to HERA of the background conditions during injection and when the backgrounds were too high to allow the CJC HV to be switched on. Occasional beam losses and other incidents resulted in the corruption of the software stored in the frontend control chips. This then had to be reloaded, implying the radiation monitor was off for short periods. More seriously, some of the above-mentioned incidents caused damage to circuits in the repeater electronics, which is located at the outer BST pad detector radius (*i.e.* at about 12 cm from the beam axis). Such problems were not observed prior to 2002. The damaged repeater electronics will be replaced during the coming shutdown. Laboratory measurements will also be made in the shutdown, for example of leakage currents, and will provide more detailed information on the nature of the damage caused to the BST pad and strip detectors and their electronics. It is already apparent

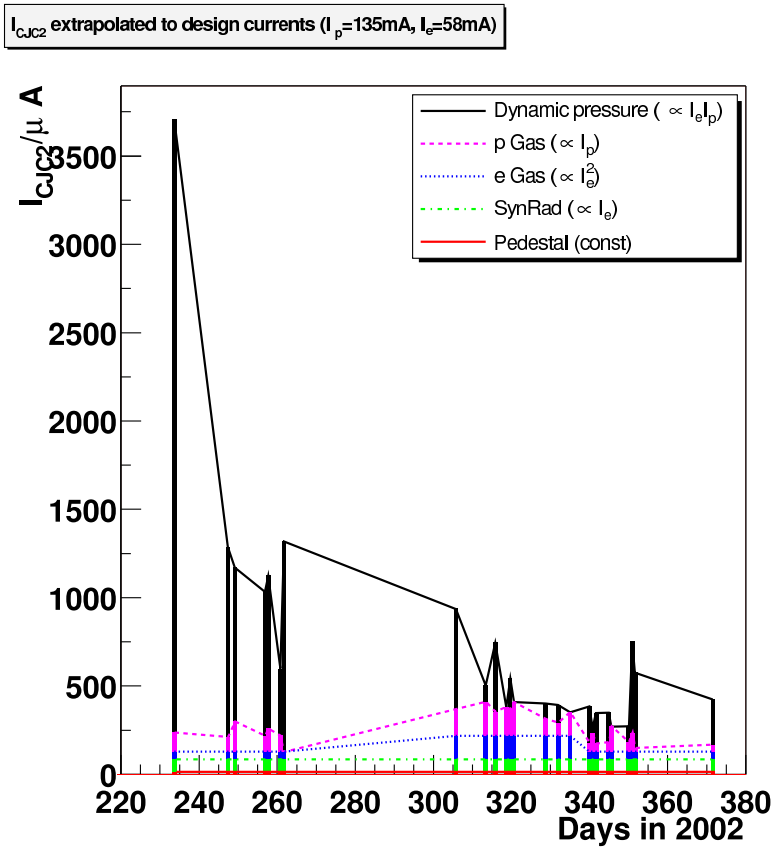

Figure 18: Currents in the outer drift chamber, CJC2, as a function of time. Shown is a decomposition of the contributions from synchrotron radiation, e-gas and p-gas interactions (the a_i in equation 2). All contributions are scaled to the HERA II design currents, $I_e = 58$ mA and $I_p = 135$ mA. The CJC current limit is about $200\,\mu$A.

that damage has occurred to both the strip and the pad repeaters that are located at the same ϕ positions. These are independent boards mounted on top of each other.

Further information on the dose delivered to the BST will be obtained in the shutdown when the film dosimeters attached to the device are evaluated. These are taped to the BST at the positions shown in figure 19. The doses determined from similar dosimeters in the years 1998 and 1999 and in the year 2000 are shown in figures 20 and 21 respectively. Backgrounds in the 1998 and 1999 running were larger than in 2000. The integrated dose seen by the BST pad detector is shown in figure 23. The monthly dose was estimated to correspond to about $100\,$rad, about 30 to 50% of which was absorbed in relatively short background "spikes". The measurements in September and November were made at different ϕ positions as the detector used in September became inoperable due to the accidents mentioned above. It is not clear what dose was delivered to the detector in this incident, however, the dose delivered to parts of the BST in 1998 . . . 1999 was about $40\,$krad (*c.f.* figure 20) and despite this no malfunctions were observed. This suggests that a considerably larger dose must have been absorbed in 2002 to cause the difficulties described in the above.

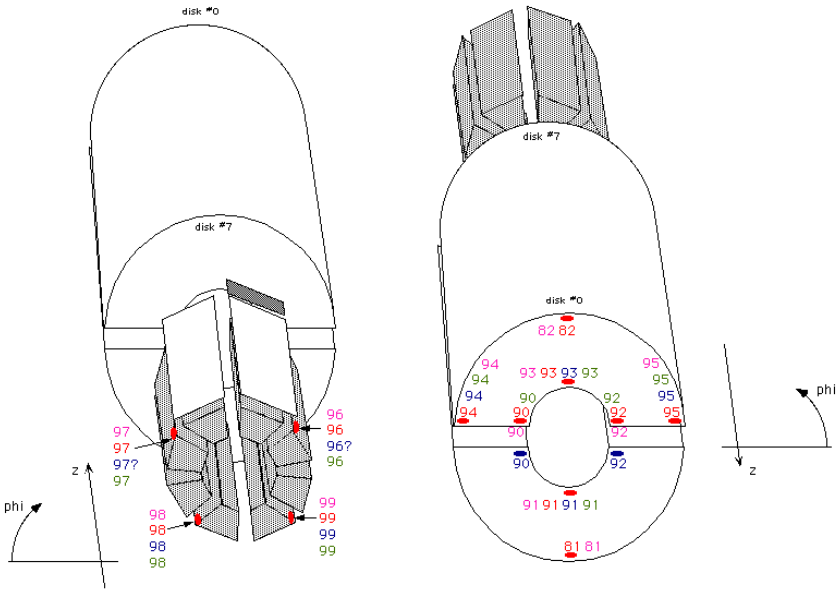

Figure 19: The positions of the various film dosimeters attached to the BST.

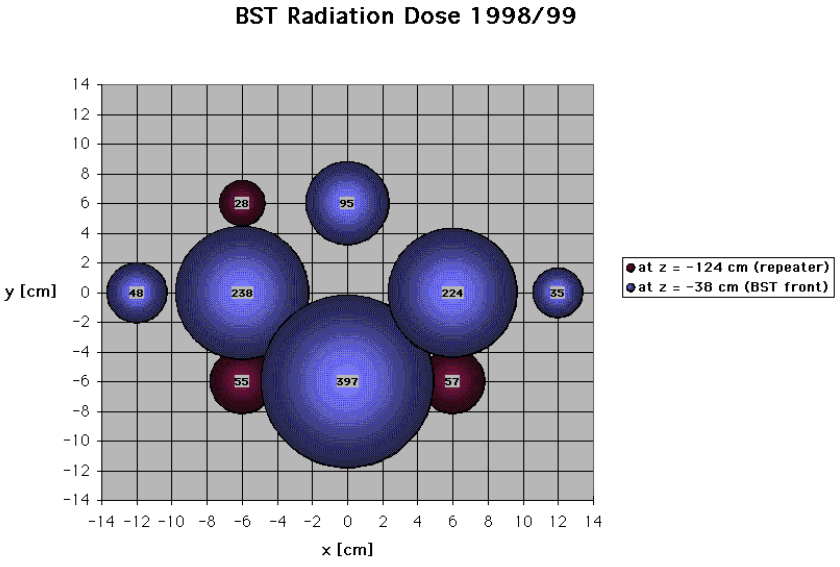

Figure 20: The radiation levels recorded in Grays in the dosimeters attached to the BST during the 1998 and 1999 running during which the backgrounds were high (1 krad$=10$ Gy).

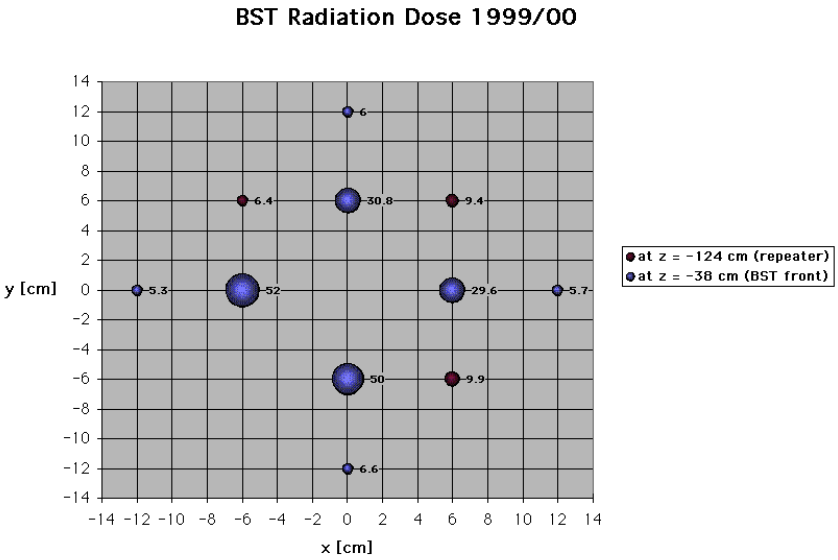

Figure 21: The radiation levels measured in Grays in the dosimeters attached to the BST during the running in the year 2000 during which the background situation was good (1 krad$=10$ Gy).

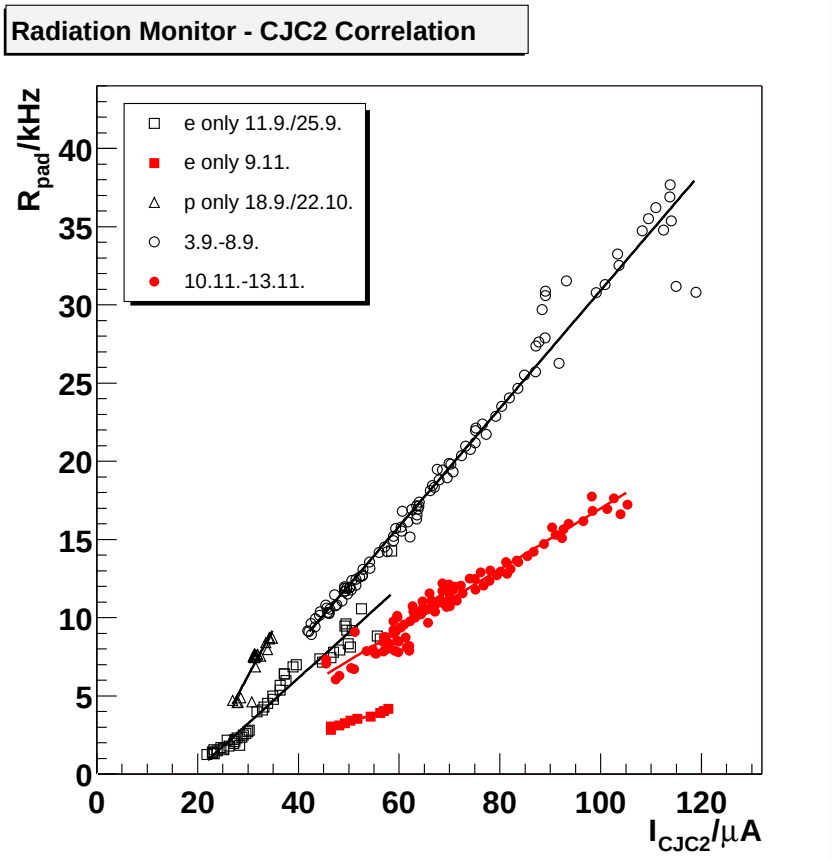

Figure 22: Correlation of the rate measured in the radiation monitor with the current drawn by the CJC2 for various fills during ep, p only and e^+ only running in 2002. On November 4^{th}, the pad sensor used as radiation monitor was changed due to a malfunction of the original sensor related to radiation damage that occurred during a partial beam loss. The new sensor is at a different ϕ position to the original and, for given beam conditions, measures only half the rate of the original detector. The November data thus lie below those taken in September. The dose received by the detector in the incident on the 4^{th} November is not known.

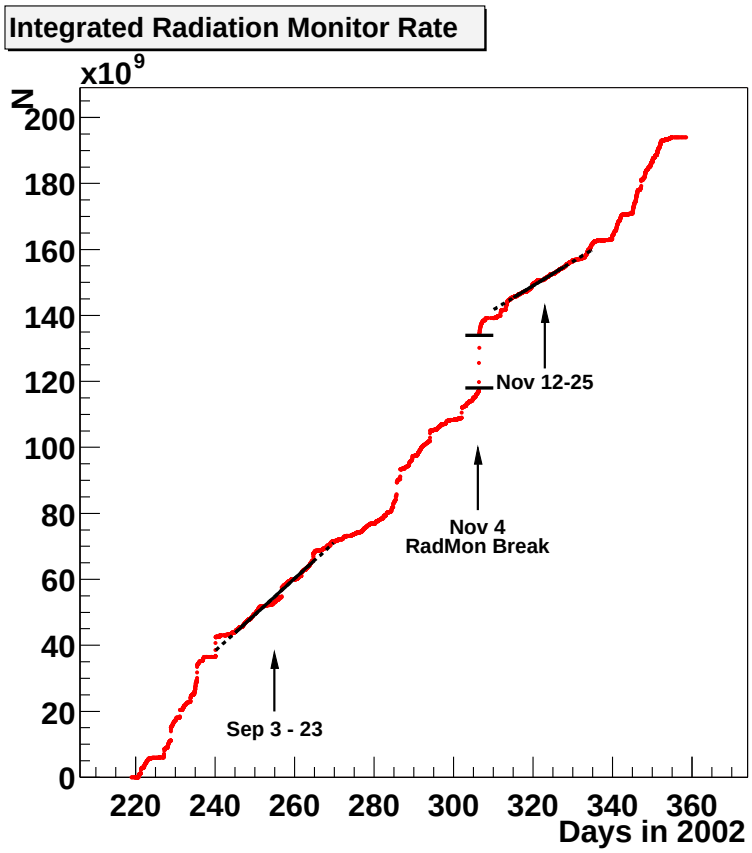

Figure 23: Integrated rate observed by the H1 silicon pad detector in 1/16 of 2π during the autumn 2002 HERA run. A monthly dose of about 100 rad was received, calculated from the slopes at the positions indicated, with unknown additional contributions from radiation accidents.

3 Further background studies

3.1 Study of source of poor vacuum

The above studies, *e.g.* figure 18, and those reported in [1], suggest that proton-induced background will be the dominant problem in H1 at HERA design currents, and that the rate of primary proton beam-gas interactions increases strongly with positron current due to desorption of gasses from the surfaces within the vacuum chambers. This section describes measurements made in an attempt to further understand the possible sources and mechanisms underlying this process. These include attempts to identify potentially "dirty" components within the beam line, to determine experimentally within which regions along the beam line H1 is most sensitive to bad vacuum conditions and to localise the primary proton beam-gas interactions responsible for the backgrounds in H1.

3.1.1 Warming absorbers

A potential source of gas close to the H1 detector is the absorber at $z \approx -3.6\,\mathrm{m}$, Abs 1. There was some concern that this may have been contaminated during machining and that outgassing was then occurring, particularly during injection when the temperature of the absorber may be relatively high. In order to test this hypothesis, the absorber was heated up to a maximum temperature of $80\,\mathrm{C}$ by pumping hot water through the cooling circuits while a mass spectrometer was connected at the nearest available port at $z = -26\,\mathrm{m}$. The spectra recorded before and during heating are shown in figures 24 and 25, respectively. Both spectra show the presence of methane ($A = 16$), water ($A = 18$) and carbon monoxide ($A = 28$). There is no evidence for the appearance of additional heavy components in the spectrum during heating, as might be expected if Abs 1 was contaminated with lubricants or coolants. A note of caution must be sounded, however, as there are many vacuum pumps between Abs 1 and the port at which the mass spectrometer was connected. It is possible that some contaminants would fail to get past these and hence would not be registered in the mass spectra.

3.1.2 Heating of titanium sublimation pump at NR 3.6 m

Heating of TSPs is used to locally degrade the vacuum in a controlled way and to observe how this local change of pressure influences the background in the detector. During a proton only run on November 28$^{\mathrm{th}}$, the TSP at NR 3.6 m ($z = -3.6\,\mathrm{m}$) was heated in several steps. The pressure measured in the adjacent ion getter pump increased by a factor of approximately 200 from $1.3 \times 10^{-9}\,\mathrm{mbar}$ to $3 \times 10^{-7}\,\mathrm{mbar}$, while the pedestal subtracted currents in CJC2 and CJC1 increased by factors of 20 and 25 respectively, as illustrated in figure 26. Heating the pump close to the H1 detector results in the released gas propagating into and through the H1 beam pipe; a pressure increase was also noted on the opposite side of the H1 detector at the pump at NL 6 m, as is also shown in the figure.

The increase in chamber currents initially seems rather small, given the large increase in pressure, and would appear to suggest that high pressures close to the experiment cause little proton-induced background. However, laboratory measurements of the heating of a TSP similar

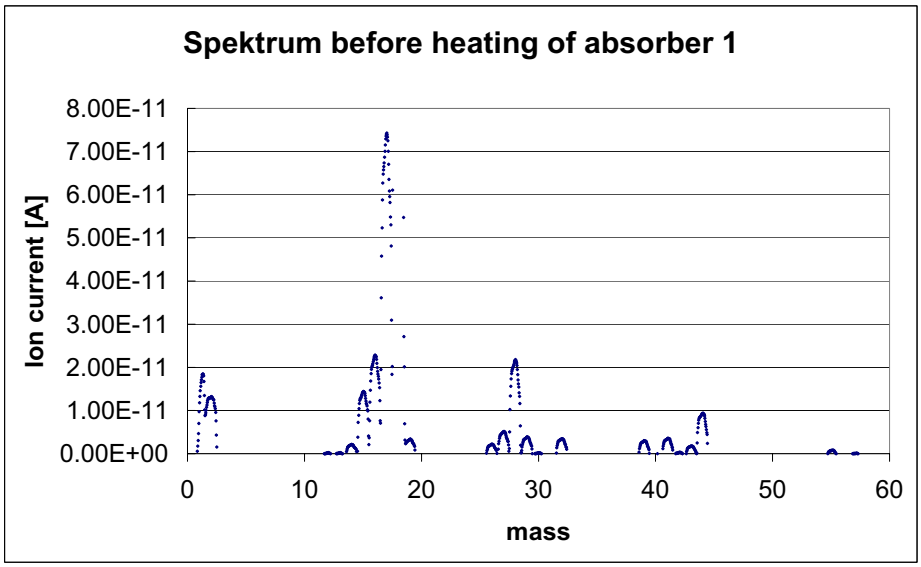

Figure 24: Mass spectrum taken at NR 26 m before warming of absorber 1.

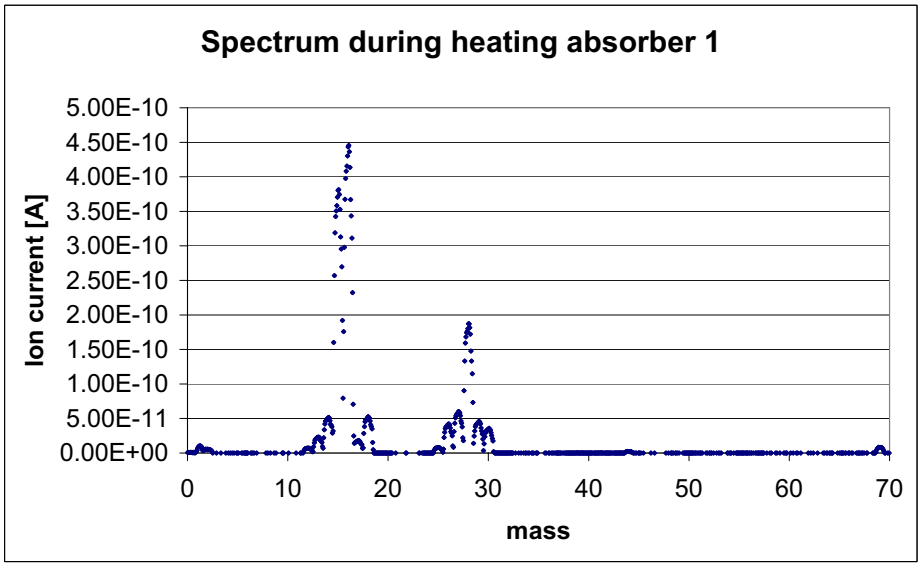

Figure 25: Mass spectrum taken at NR 26 m during warming of absorber 1.

to that at NR 3.6 m [3] revealed that, with the heating regime used here, it is mainly hydrogen that is released from the pump. The effect on the background of a large pressure increase can then be relatively small, given that the residual gas under normal conditions is of considerably larger molecular weight than hydrogen, *c.f.* figure 8, and that the cross section for the interaction

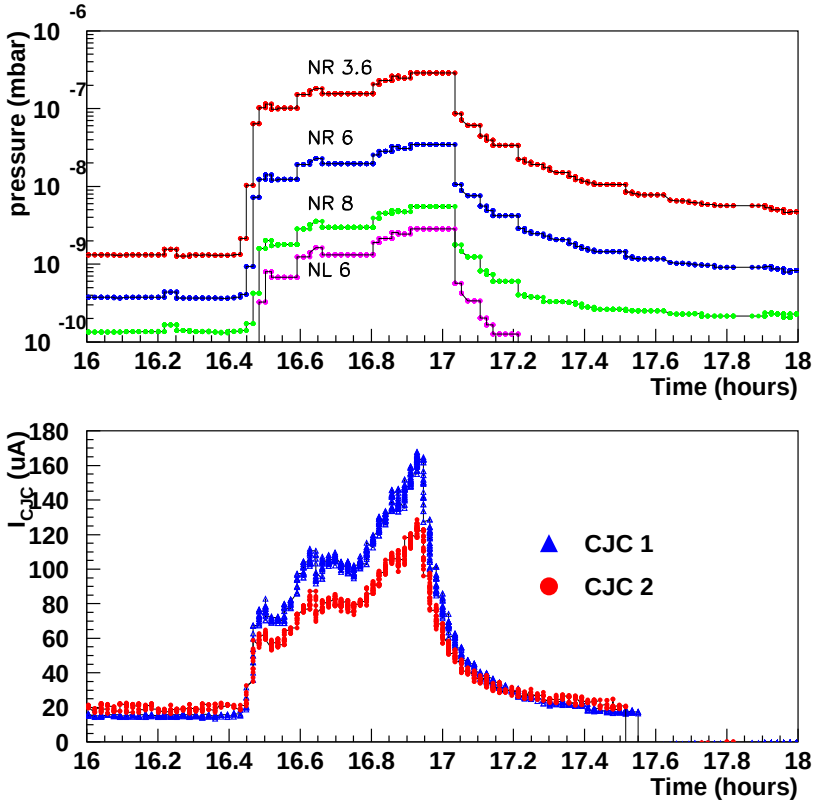

Figure 26: Top: pressure development during the heating of the TSP at NR 3.6 m on November 28$^{\text{th}}$ 2002. Bottom: CJC current history.

of protons with hydrogen nuclei is smaller than that for interactions with heavier species.

Confirmation of the above was obtained by studying the charged multiplicity distribution during the pump heating exercise. The multiplicity before and during/after the heating is shown in figure 27, together with the expectations for the multiplicity arising from proton interactions with various gasses. The multiplicity is observed to decrease significantly following the heating of the pump. Whereas before the heating the multiplicity is compatible with that expected for a gas of molecular weight similar to water, following the heating it agrees better with the expectations for a gas composed of 50% H_2O (or compounds of similar molecular weight such as CO) and 50% H_2.

In order to check if the approximately twenty-fold increase in chamber current is quantitatively consistent with the observed pressure increase of a factor of about 200, a comparison of the measured ratio of the event z-vertex distributions for beam gas events during and before the heating was made with the expectations arising from a model which describes at least approximately the observed pump readings left and right of the detector [4]. The model is based on the calculated gas conductances of the vacuum chambers close to H1, the pumping speeds of the pumps for various gasses and assumptions about the outgassing rates from the vacuum chamber walls. Figure 28 shows the result of this comparison, which is made under the assumption that the dominant gas component before heating is carbon monoxide while it is hydrogen during the heating. There is very satisfactory agreement between the two distributions given the fact that there are still significant uncertainties in the model assumptions for conductances, pumping speeds, pump sensitivities *etc.* Further refinements of the model will allow more detailed

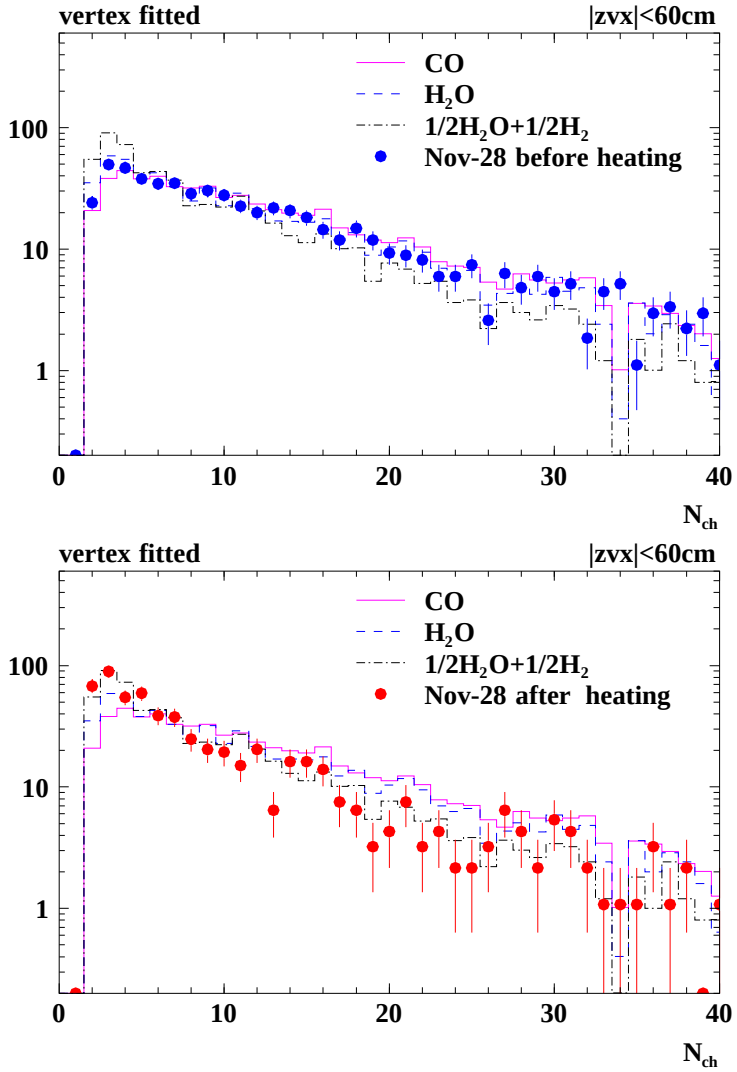

Figure 27: Charge multiplicity distributions before (top) and during/after (bottom) heating of the TSP at NR 3.6 m. Also shown are Monte Carlo expectations for proton interactions in various gasses.

comparisons to be made.

3.1.3 Heating of further titanium sublimation pumps

Having understood the behaviour of the TSPs when heated and the response of H1 to the resulting pressure increase, it becomes possible to experimentally investigate the sensitivity of the CJC to primary proton beam-gas interactions as a function of their distance from the detector. This was done by heating a succession of TSPs, with proton beams in HERA, and observing the resulting pressure increases and the changes in the CJC currents. Figure 29 shows the correlation between P_{max}, the maximum pressure measured in the ion getter pumps adjacent to the heated TSPs, and the resulting change in the CJC1 current, ΔI_{CJC1}, normalised to the proton beam current. The values of P_{max} were in all cases significantly larger than the base pressures

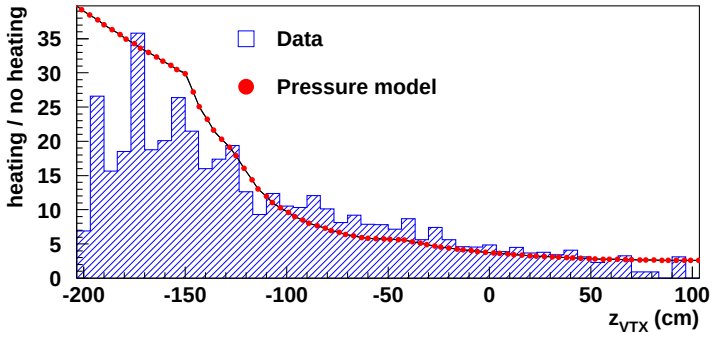

Figure 28: The ratio of distributions of the beam gas event z-vertices during/after and before heating the TSP at NL 3.6 m. The circles show the prediction from a model designed to describe the pressure changes within H1 during the heating exercise.

at the positions of the pumps, ensuring that P_{max} is a measure of the pressure change induced by the heating process.

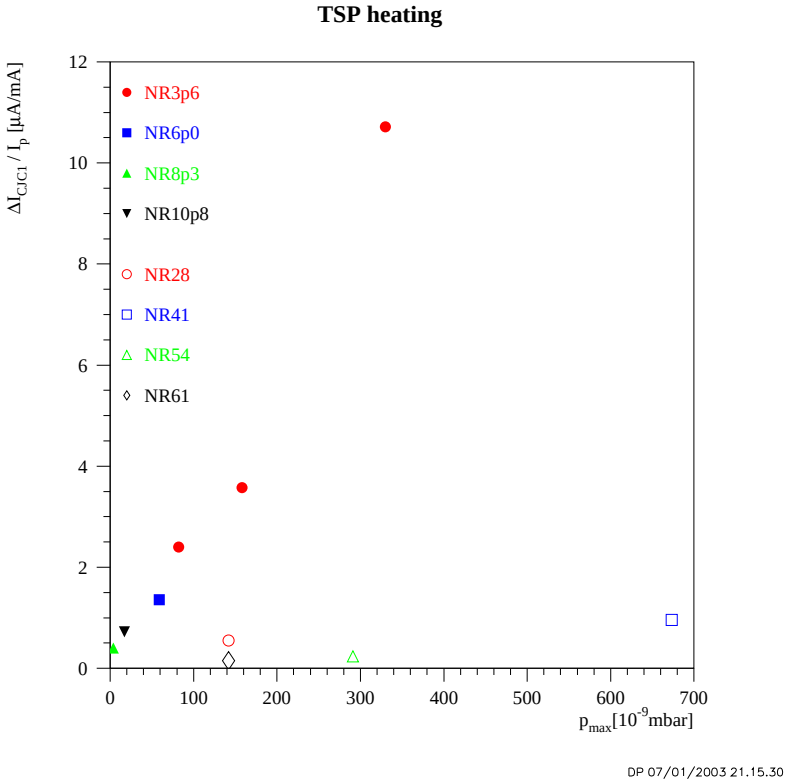

Figure 29: The correlation between the maximum pressure induced by heating various TSPs and the resulting change in the current drawn in the CJC, normalised to the proton beam current.

Figure 30 shows the sensitivity of the CJC1 to the pressure bumps induced by the TSP heating as a function of z. Plotted is the change in the CJC1 current per unit pressure change, normalised to the proton current. The measurements are compared to a prediction made using the proton beam-gas Monte Carlo described in [1] under the assumption, justified by the above,

that the gas released when the TSPs are heated is primarily hydrogen. Reasonable agreement is seen, particularly when it is borne in mind that the systematic uncertainty in the measurements is at least 20%, as is illustrated by the spread of the three measurements taken at $3.6\,\mathrm{m}$, each with different values of P_{max}. Further, the geometry of the pumps in the range 11 to $61\,\mathrm{m}$ is such that the getter pump sees a larger proportion of the pressure induced in the heating of the TSPs than do the getter pumps closer to H1. The more distant values should thus be corrected upwards somewhat.

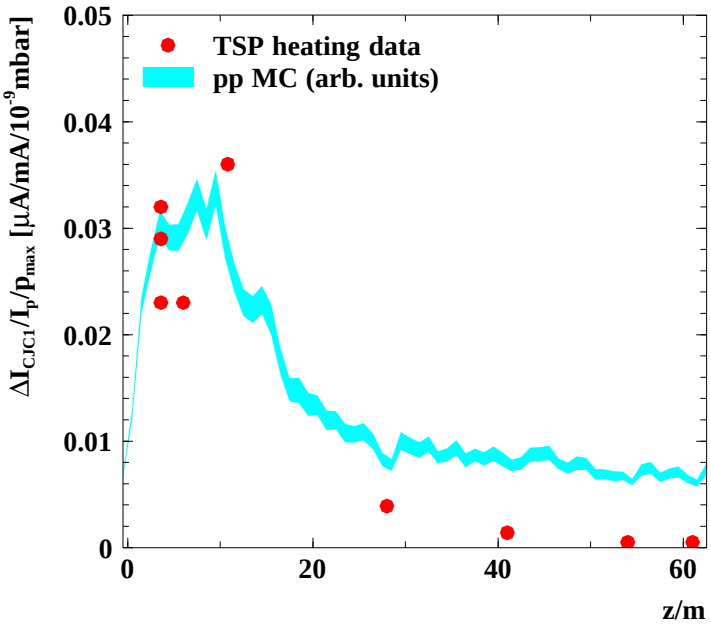

Figure 30: The sensitivity of the CJC currents to changes in the pressure in the beam line induced by heating the TSPs, shown as a function of the position along the beam line up to $z = -60\,\mathrm{m}$ from the H1 detector for proton only operation. The points represent the data while the band is a Monte Carlo prediction assuming that heating the TSPs leads to the production of hydrogen.

3.1.4 Switching off pumps

Experimental measurements of the sensitivity of the H1 detector to deterioration in the vacuum at different positions along the beam line may also be made by turning off selected ion getter pumps. This was attempted for the pump at NR 3.6 m. The results are shown in figure 31. There is no perceptible change in the CJC current during the period in which the high voltage of the getter pump was off. It is, however, likely that the pressure change resulting from switching off the getter pump was small. Firstly, the pumping speed of the getter pump is small compared to that of the TSP at the same location, $60\,\mathrm{l/s}$ as opposed to $1000\,\mathrm{l/s}$, and secondly, the getter pump continues to function as a titanium sublimation pump even when turned off until the titanium surfaces become saturated; this may take hours or even days depending on the pressure. Despite this, the pressure measured at NR 6 m is seen to rise slightly. It is possible that this is due to methane, which is not efficiently pumped by TSPs. This experiment was considered inconclusive due to the various difficulties mentioned above and was therefore repeated using

pumps close to the ZEUS experiment, which were left off for a considerably longer time than those at H1. The results are presented in the ZEUS background report [5].

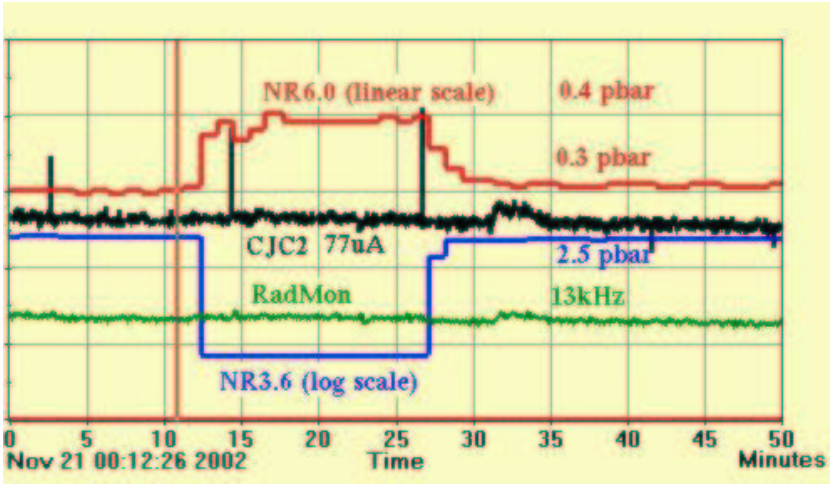

Figure 31: The current in CJC2 and the radiation monitor rate shown as a function of time together with the voltage applied to the getter pump at NR 3.6 m and the pressure measured in the getter pump at NR 6 m.

3.1.5 First measurements with Backward Tagging System

During a HERA maintenance day in November, two pairs of scintillators, interleaved with 2 mm of lead, were installed as close as possible to the beam pipe at the positions of Abs 2 ($z = -6$ m) and Abs 3 ($z = -8$ m). This detector is referred to as the Backward Tagging System (BTS) in the following; its purpose is to aid localisation of the primary interactions responsible for the proton induced backgrounds within H1. A "hit" in the BTS was defined to be the logical OR of the coincidence of each of the pairs of scintillators. The observation of a hit in the BTS followed by a p-gas background event in the CJC provides some indication that the event originated from further upstream along the proton beam line than the BTS, *i.e.* from the region with $z < -6 \cdots -8$ m. Positron induced events cause an event in the CJC with a subsequent hit in the BTS if the positron showers and causes a signal in the scintillators. Both signatures may be confused by the presence of accidental coincidences.

First studies of the location of the primary vertices of the events responsible for the proton-induced background were made using the BTS in coincidence with the DCrφ trigger. Figure 32 shows vertex distributions for events in which there was a DCrφ trigger in coincidence with a BTS signal in the time window expected if a proton caused the primary interaction (BTS-p, upper plots) and with a BTS signal in the time window expected if an electron caused the primary interaction (BTS-e, lower plots).

From the distribution of the vertices in x and y in the upper left plot, one can see that the requirement of a BTS-p signal removes all the events with origins around the nominal beam line ($x \simeq 0.4$ cm, $y \simeq 0.6$ cm) from the sample which are otherwise clearly observed in DCrφ triggered events, *c.f.* figure 39 in [1]. Events at the beam position come from proton-gas interactions inside the H1 detector and from ep interactions. Events with vertices removed rom the beam position are from secondary interactions with the beam wall and the collimators C5B

and C5A. The absence of beam gas events in the BTS-p sample confirms that the rate of random coincidences is small. If coincidences between a DCrφ and BTS-e signal are required, predominantly genuine ep events are selected, as can be seen in the lower part of the figure in which prominent peaks are visible in both the x-y plane and in z around the nominal interaction position. Studies now underway with this new detector will provide information on the location of the primary interactions responsible for a large proportion of the H1 backgrounds. In addition, the possibility of operating scintillators further along the proton beam line is under investigation.

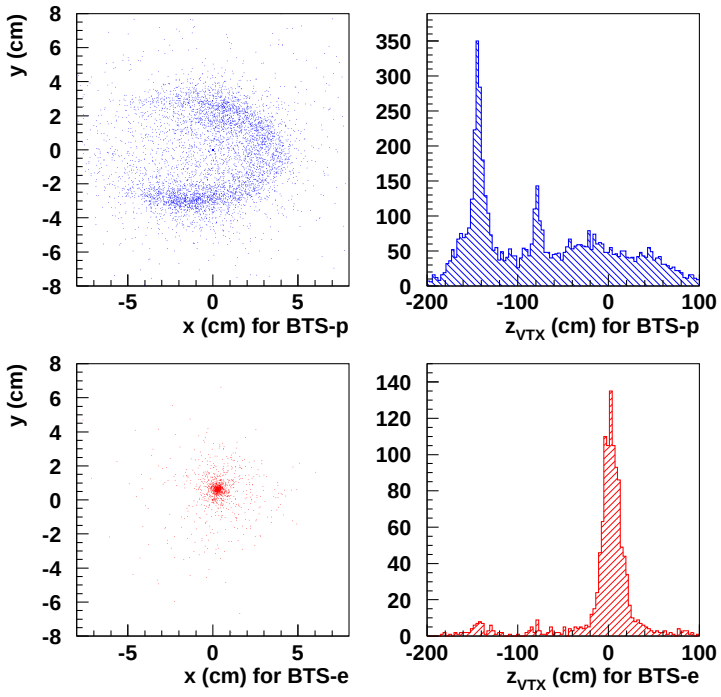

Figure 32: Position of reconstructed CJC vertices in x-y (left) and z (right). Top: events triggered by the coincidence of DCrφ and BTS-p are from secondary interactions with the beam pipe or collimators. Bottom: events with BTS-e signal and DCrφ trigger are dominated by genuine ep interactions.

3.1.6 First Forward Silicon Tracker measurements

The Forward Silicon Tracker (FST) consists of 5 silicon wheels, each of which is composed of two single-sided silicon strip detectors mounted back-to-back. The wheels are oriented perpendicular to the beam pipe, have a sensitive radius which extends from about 6 to 12 cm and are spaced uniformly along the beam pipe in the range $35.8 < z < 51.2$ cm. The detector signals are stored in a capacitor pipeline amplifier (APC128) and are read out using repeater electronics located in front of the most forward wheel at a radius of about 14 cm. The FST is connected via a contact ring to cables and cooling water pipes which lead to the H1 electronics trailer. It was installed during the luminosity upgrade and is designed to improve the acceptance of H1 for heavy flavour and high Q^2 physics in the forward region. The FST was operated throughout the latter quarter of 2002. Here, it is used to reconstruct tracks near the beam axis which originate from in front of (towards larger z) and behind (towards the IP and smaller z) the detector,

i.e. from e-gas interactions at $+z$, from ep interactions near $z \simeq 0$ and from p-gas and p-wall interactions at negative z.

Figure 33 shows the distribution of the origin in z of FST tracks measured in luminosity running (top) and in a proton only run (bottom). The coordinate shown, z_{FST}, is the z value at which the helix reconstructed from the FST measurements approaches most closely the nominal beam line. One observes a dominant peak from ep interactions, a significant amount of proton background at negative z values and some tracks from positive z. The relative importance of the different contributions is dependent on the triggers used in these runs. For comparison, and to allow studies of the proton background, figure 33 (bottom) shows the z_{FST} distribution from a proton only run, with the same triggers, in which the ep peak and the e-gas contribution are not present.

Figure 34 summarizes characteristics of the proton background tracks reconstructed in the FST, where the tracks are defined using at least 4 space points in the FST. The signal-to-noise ratio of the hits associated with these tracks is, as in ep events, very high, *i.e.* the most probable value is about 30, the Landau distribution being truncated by the 6-bit representation of the S/N in the on-line readout of the detector. Most of the background tracks have small transverse momenta, typically a few 100 MeV and are distributed in momentum as shown in the figure.

The FST tracks are of interest here as they provide information on the origin of proton initiated background over a larger region than accessible with the H1 drift chambers. Monte Carlo studies show that the FST geometry and the fields of the HERA beam magnets limit the range in which z_{FST} is well correlated with the origin in z of proton beam-gas interactions to $0.4 > z > -4$ m. The ratio of the ep to p only event distributions in this range is shown in figure 35 (top). This ratio is independent of the geometric acceptance of tracks in the FST, as discussed below. Apart from the ep event peak around the nominal interaction vertex, it is seen to be rather flat. This suggests that none of the beam line elements, such as absorbers and collimators, are causing dramatic HOM heating which would lead to local pressure bumps and cause bumps in the proton beam-gas rate during ep running which would then be visible in the above ratio.

The Monte Carlo was used to reconstruct the true z vertex distribution of the primary proton beam-gas interactions from the measured z_{FST} distribution. A smeared acceptance was defined as the ratio of the distribution of z_{FST} to the distribution of true vertices. This corrects for the geometric variation of the acceptance with z, which increases by about a factor of 20 from -4 m to -1 m. Correcting the measured z_{FST} distribution, figure 33 (bottom), for the acceptance and z smearing effects yields the true z vertex profile as shown in figure 35 (bottom). This is rather flat. Note that in this unfolded distribution the narrow peaks due to scattering in the collimators C5A at -0.8 m and and C5B at -1.5 m are visible. The next step in the FST analysis is to develop a 3D vertex reconstruction which will allow the separation of p-gas and p-wall interactions and hence enable conclusions about the pressure profile close to the IP to be drawn.

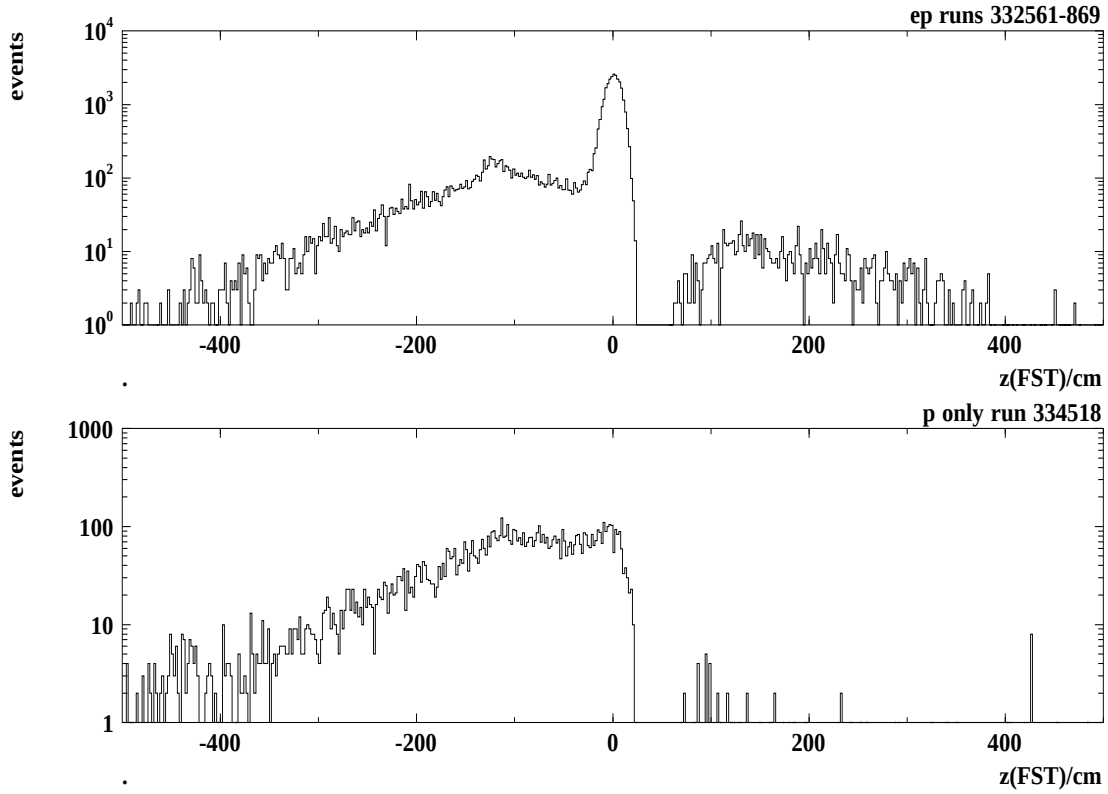

Figure 33: Distribution of z position at which tracks measured in the FST most closely approach the beam line in luminosity mode (top) and for a single proton beam run (bottom).

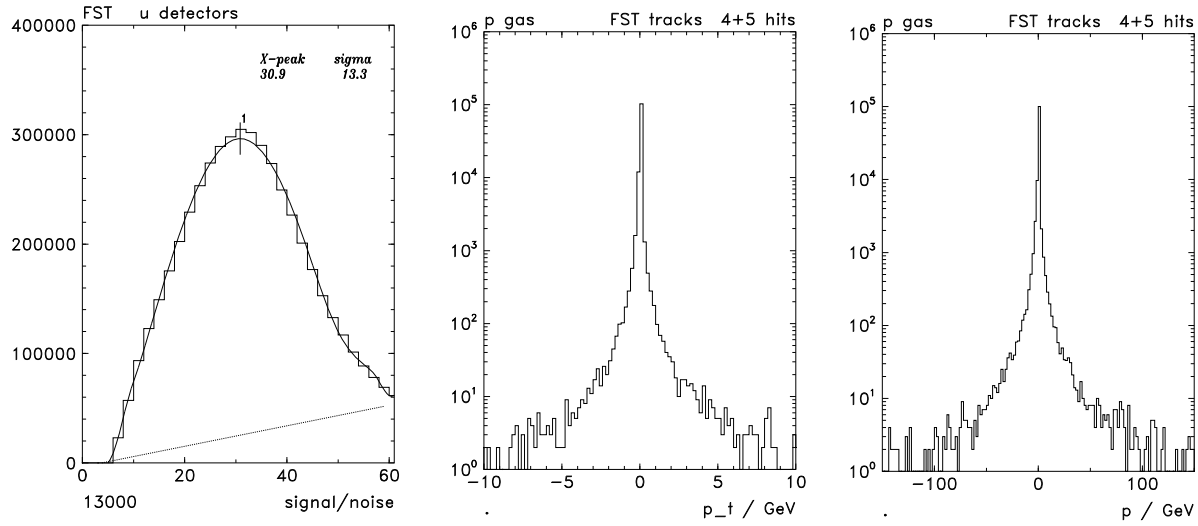

Figure 34: Characteristics of tracks measured in the FST from p only events: the signal-to-noise ratio (left), the transverse momentum for negatively and positively charged tracks (middle) and the momentum for negatively and positively charged tracks (right).

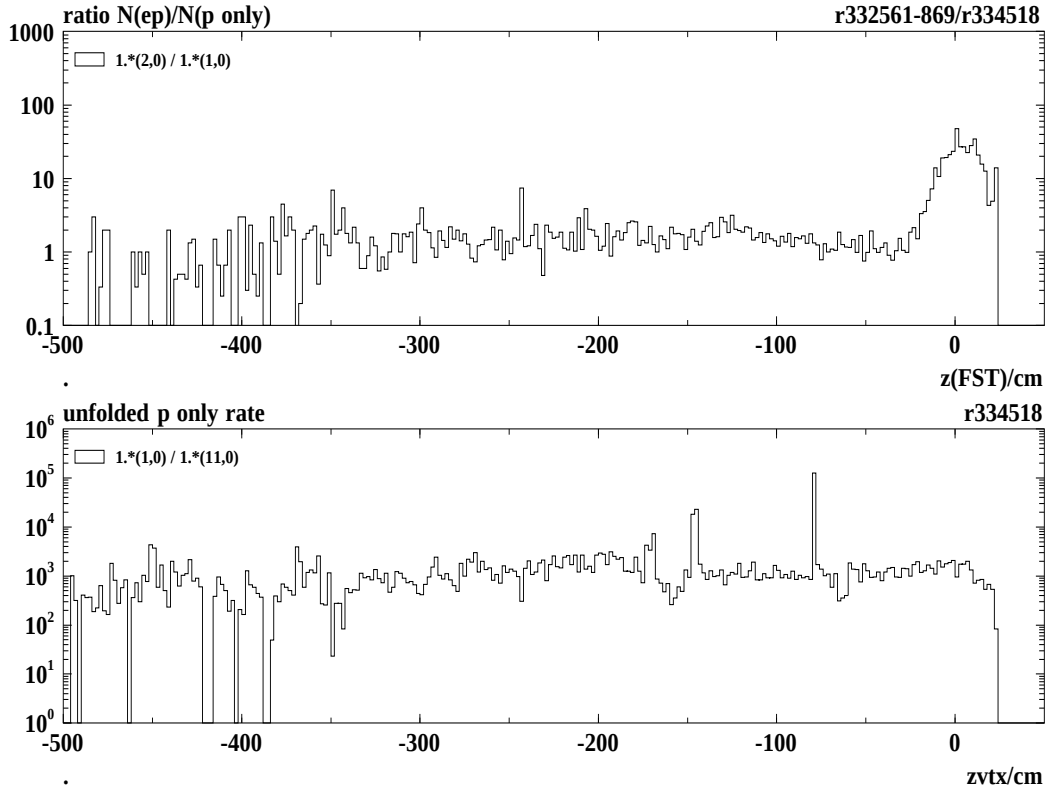

Figure 35: Ratio of distribution of z position at which tracks measured in the FST most closely approach the beam line in ep events to same distribution for p only events (top) and unfolded position of proton background event z vertices (bottom).

3.2 Investigation of effects of beam pipe temperature

3.2.1 Running with various GO and GG beam pipe temperatures

One novel feature at HERA II is the cold beam pipe section close to the IP in the GO and GG magnets. This may trap gasses which are then released through the processes of thermal or photo-desorption, the former perhaps particularly at the warm-cold transition and the latter under beam operation. It was therefore decided, after a brief test on the 1$^{\text{st}}$ October 2002, to run with GG and GO shield and beam pipe temperatures of 110 K, starting on the 9$^{\text{th}}$ October. On November 12$^{\text{th}}$, the temperature was further increased to 170 K. This temperature was chosen following the study illustrated in figure 36 in which the GO and GG shield temperatures were raised while a mass spectrometer was connected to the vacuum system at NR 26 m. The rate at which methane was detected in this spectrometer peaked at a shield temperature of about 170 K. Following the period at 170 K, the temperature was again reduced to 55 K on 26$^{\text{th}}$ November, see figure 37.

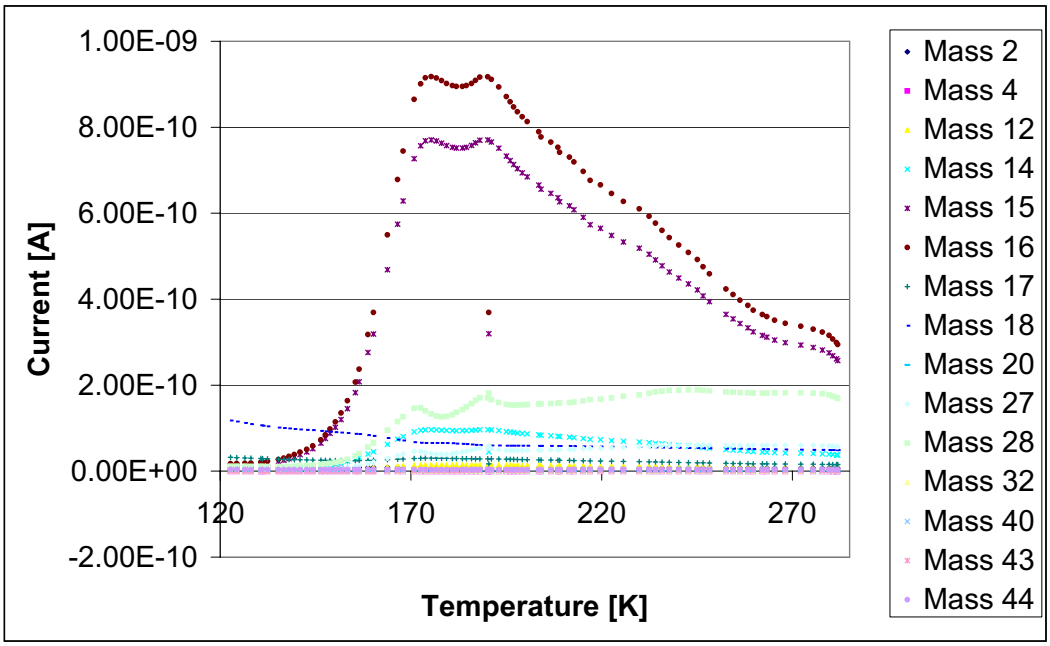

Figure 36: The rate of emission of gasses of various molecular weights as a function of the GO and GG shield temperature, measured at a distance of 26 m. The rate of emission of methane (uppermost line) is seen to peak at about 170 K.

The CJC drift chamber current history going back to April 2002 is shown in figure 38 using the September 2002 fit as a reference, *c.f.* table 1. The points are selected mainly from the

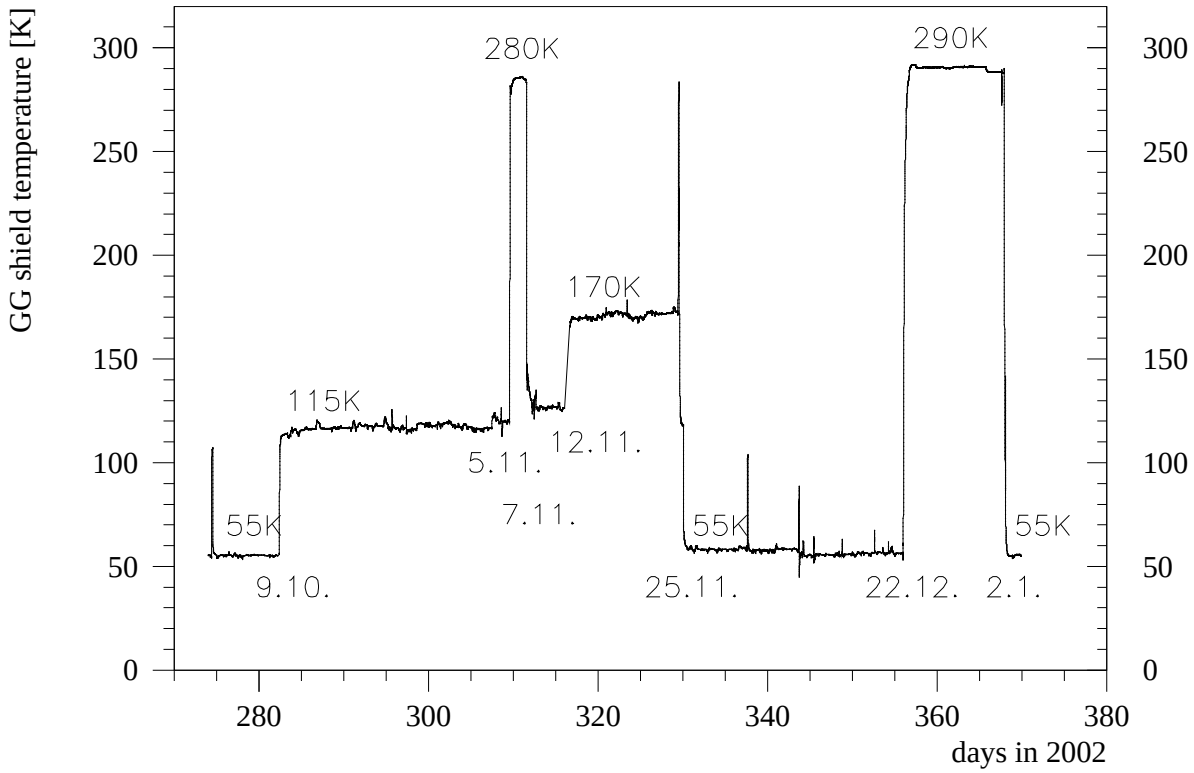

Figure 37: GG shield temperature in October, November and December 2002. The dates of the various temperature transitions are indicated. The history of the GO shield temperature is the same as the GO and GG helium supplies are connected in series.

early parts of luminosity fills, after completion of the initial beam steering period. An overall improvement by more than a factor of 10 is observed. The period with increased GO/GG shield temperatures saw rather high CJC currents, in contrast to the global trend. This may hint at a beneficial cryogenic pumping effect of the cold surfaces within GG and GO.

3.2.2 Beam pipe temperature and Higher Order Mode heating at positron injection energy

The positron beam is injected at an energy of 12 GeV and at this energy the bunches are shorter than they are following ramping to higher energies. They are thus more likely to excite higher order modes in the electron ring, which may cause local heating and possibly outgassing. Evidence for this is shown in figure 39, in which an exponential rise of the rate of Bethe-Heitler events caused by scattering off the residual gas in the H1 beam pipe is observed during injection. As expected, such a pressure increase causes a rise in the proton induced background measured in the H1 detectors, shown here in terms of the radiation monitor rate in figure 40. The proton current during the above positron injection was 21 mA.

Higher order mode (HOM) losses occur where the diameter of the beam pipe changes, forming a cavity in which the beam may excite resonances. Locations in and around H1 where such changes in diameter occur include around the collimators, *e.g.* C5a and C5b at $z = -0.8$ and -1.5 m, respectively, and in the adjacent bellows at the end of the GG magnet. In order to investigate possible HOM heating at the latter location, the bellows were equipped with a

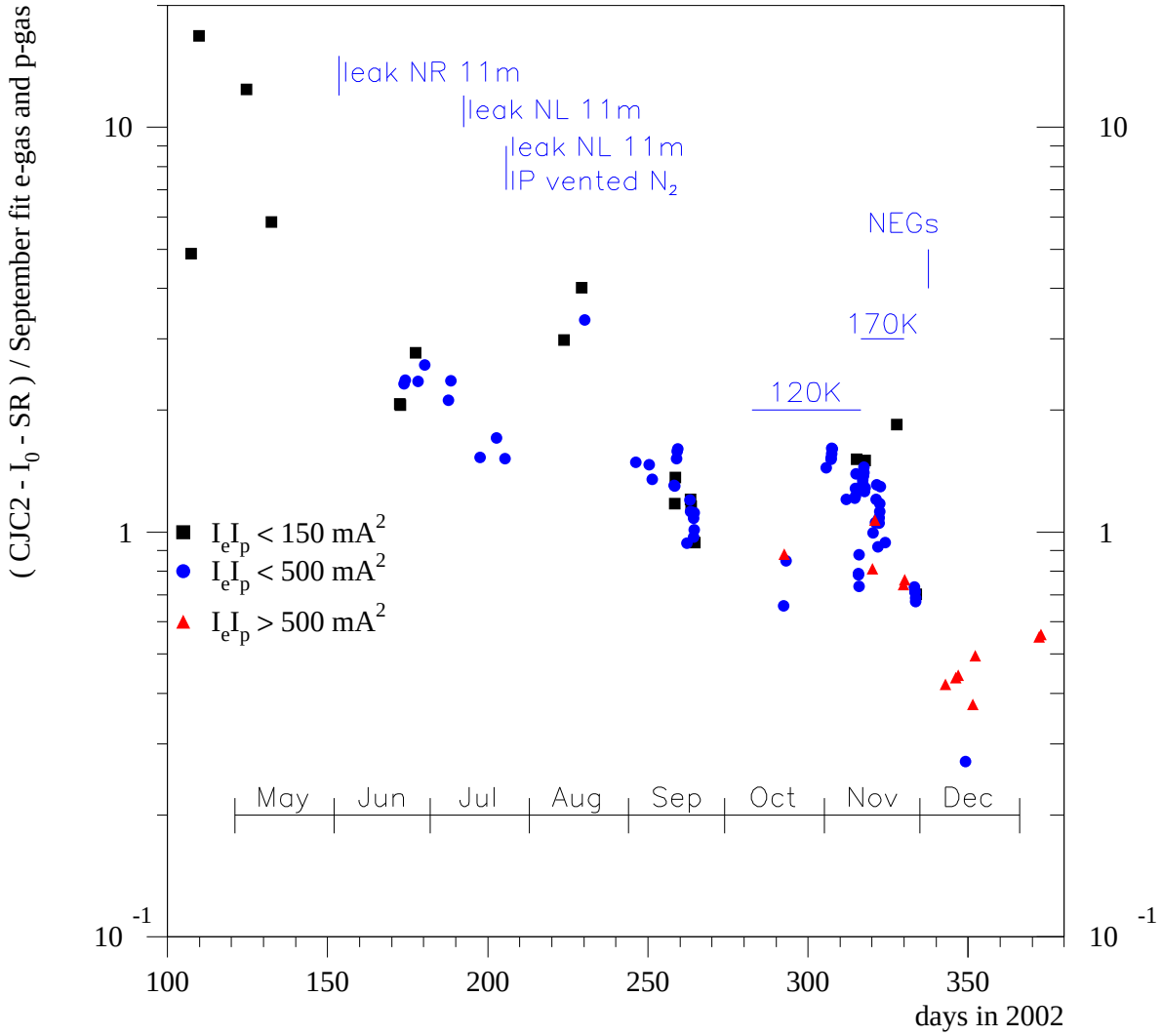

Figure 38: CJC2 current history. The dependence on beam currents is taken into account by normalizing to the e-gas and p-gas contribution from the September fit. The constant pedestal current and the expected synchrotron radiation contribution are subtracted from the measured current. The different symbols reflect the product of the HERA beam currents.

temperature sensor. The temperature recorded in this sensor is shown in figure 41. It is seen to climb as the positron beam current increases.

The significance of the HOM heating effects observed at injection becomes apparent when the resulting temperatures are compared with those seen during running at nominal beam energies, where the contribution to heating due to synchrotron radiation is much larger. Such a comparison is shown in figure 42. The temperature during injection is seen to be higher than that at nominal beam energies for all beam currents.

High temperatures resulting from HOM heating during the injection process may thus lead to the release of gasses that then cause poor background conditions in the subsequent luminosity running. Such temperature peaks should be reduced as far as is possible. This can be partially achieved by rapid injection; the time constants associated with the heating visible in figure 41 are of the order of 20 mins. The design of collimator C5b and of the GG bellows is being

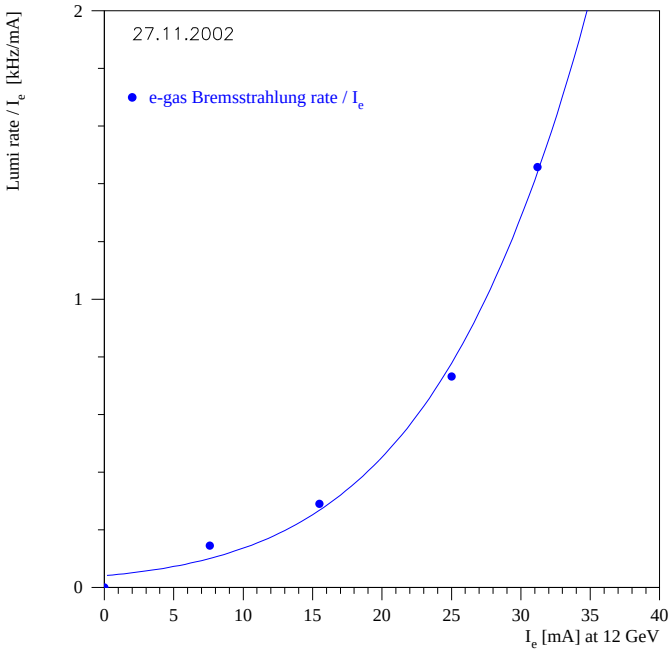

Figure 39: The rate measured in the luminosity detector as a function of positron current with a positron beam at its injection energy, 12 GeV. The rate rises exponentially with the positron current, as is shown by the curve in the figure.

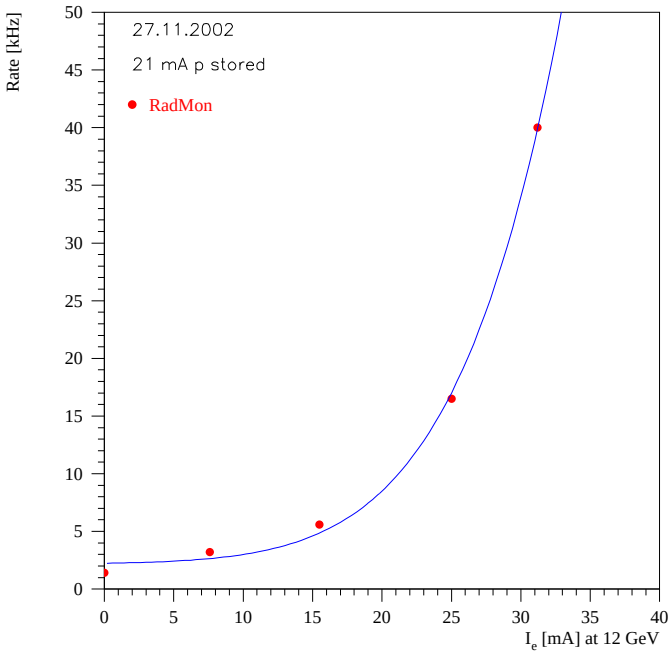

Figure 40: The rate measured in the radiation monitor as a function of positron current with a positron beam at its injection energy, 12 GeV and a proton beam of energy 920 GeV and current 21 mA. The rate observed rises exponentially with the positron current, as is shown by the curve.

modified with the effects of HOM heating in mind at both injection and nominal positron beam

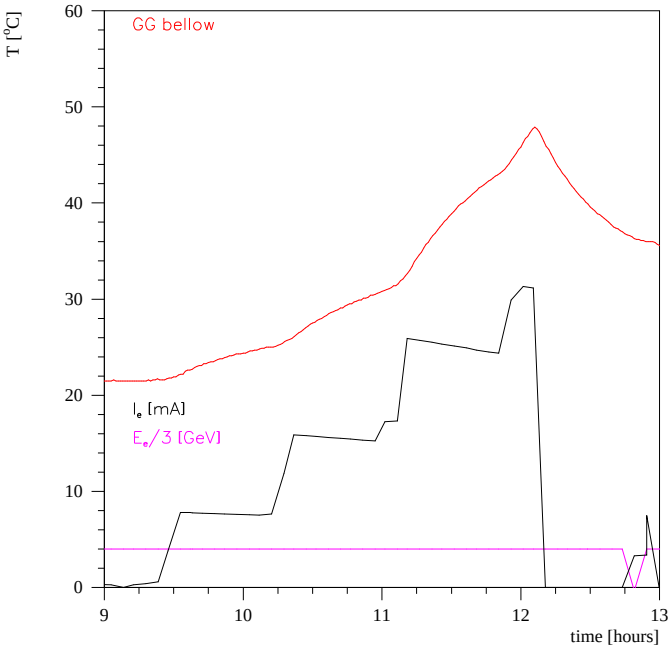

Figure 41: The temperature recorded by the sensor on the GG bellows at $z = -1.5$ as a function of time during the injection of a positron beam of energy 12 GeV, together with the beam current. The machine also contained a proton beam of energy 920 GeV and current 21 mA throughout this exercise.

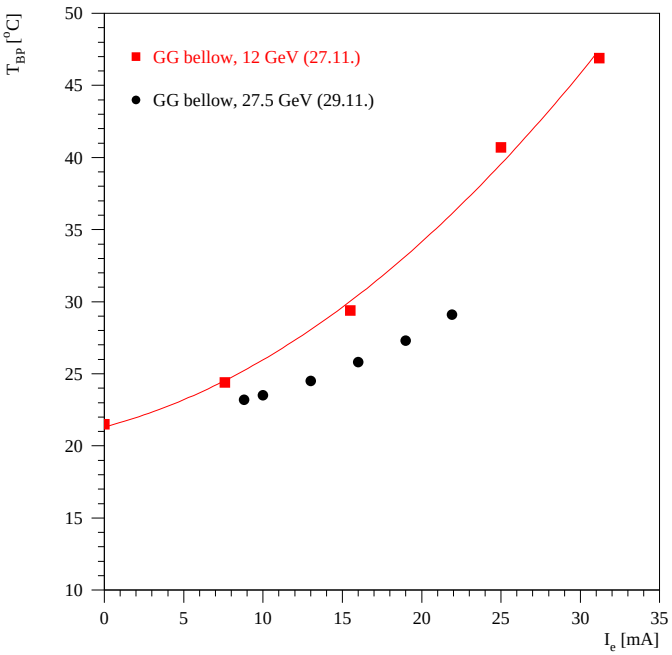

Figure 42: The temperature recorded by the sensor on the GG bellows at $z = -1.5$ m as a function of positron beam current at injections energy (12 GeV) and at nominal energy (27.5 GeV).

energies. Further improvements may be achieved by increasing the positron bunch length at injection.

3.3 Ion trapping

3.3.1 Trapped ions as a source of background

A further difference between H1 and the HERA machine before and after the upgrade is the

Figure 43: Shown as a function of time are: black stepped line, the current in the H1 solenoid (only values of current at which sampling occurred shown); blue line which peaks at 3.5 mins, rate of positron beam-gas induced Bethe-Heitler events; central dark red and pink lines, the x and y positions of the photons impacting on the photon detector of the luminosity system; green line that rises to become that highest in the plot at 12 mins, the measured luminosity; red line that rises to a central position at 12 mins, the rate measured in the luminosity system's photon detector.

configuration of the magnetic fields in and close to H1. It was conjectured that the H1 solenoid and the GG and GO magnets might form a "magnetic bottle" in which ions could be trapped. Ions are created in collisions of the protons and positrons with the residual gas and would then be trapped in the bottle, leading to an increased rate of proton and electron beam-gas interactions within the H1 interaction region. In order to test this hypothesis, the H1 solenoid was ramped down during a luminosity run. The HERA feedback and control mechanisms were able to maintain the non-colliding beams reasonably close to their nominal orbits, as is illustrated in figure 43 by the relatively stable horizontal and vertical impact positions of the photons on the luminosity system's photon detector. As is also shown in the figure, the rate of beam gas induced Bethe-Heitler events, measured using the positron pilot bunches, before and after ramping down the solenoid and therefore releasing any ions that were trapped in its field, is very similar, indicating that trapped ions do not contribute significantly to the positron beam-gas interaction rate and hence do not affect the proton beam-gas rate significantly.

3.3.2 Ion cyclotron resonance and residual gas composition

An ingenious method of determining which chemical species are present in the residual gas within the H1 experiment was proposed in [6]. The idea is that the HERA positron beam

can be used both to ionise the gas within the H1 beam pipe and to excite cyclotron motion of the resulting ions in the solenoidal field of the H1 detector. When the frequency of the cyclotron motion matches that at which the positron bunches pass through H1, a resonance occurs which may be detected through an increase in the rate of Bethe-Heitler events observed in the luminosity system. The mass of the ions involved may then be determined from the resonance frequency and the magnetic field strength. In order to realise the resonance condition, given the field strengths that can be provided by the H1 solenoid, non-standard positron bunch patterns are needed. These aim to get as close as is possible to equal bunch spacing round the HERA ring while passing through H1 with the required frequency. In order to ensure that the vacuum conditions are the same as those that pertain during normal HERA operation, similar beam currents are required. The bunch patterns necessary for resonance then imply that large bunch charges are needed. The experiment was attempted several times, but unfortunately it proved impossible to store the necessary bunch charges. The possibility remains that the residual gas composition be measured using this technique with lower bunch charges.

3.4 Positron beam-gas simulation

In order to investigate in more detail the contribution positron beam-gas interactions make to the backgrounds in H1, a Monte Carlo program has been developed within the GEANT framework. Bethe-Heitler events are simulated along the nominal beam line in the range $0 < z < 60\,\mathrm{m}$, including the effects of the beam size and divergence. The effects of the material of the magnets, beam pipe, vacuum chambers and collimators are included in the simulation, as are those of the magnetic fields. First studies indicate that this Monte Carlo is able to explain several features observed during H1 data taking. As an example, figure 44 shows results obtained during a positron only run in November, compared with the predictions of the Monte Carlo. A "hot spot" is observed in the SpaCal at positive x, *i.e.* towards the inside of the HERA ring, which is visible also in the Monte Carlo. This is due to upstream Bethe-Heitler events, in which positrons lose energy. They are then deflected by the dipole magnets into the H1 rear calorimeter. The energy spectra of these energy deposits in data and Monte Carlo are also shown in the figure and are seen to be in reasonable agreement. Further, more diffuse energy deposits are also observed in the SpaCal at negative x. These are not reproduced by the Monte Carlo. The low multiplicity peak present in the data but not in the Monte Carlo in the charged multiplicity distributions in figure 44 has been shown in previous studies [1] to be due synchrotron radiation.

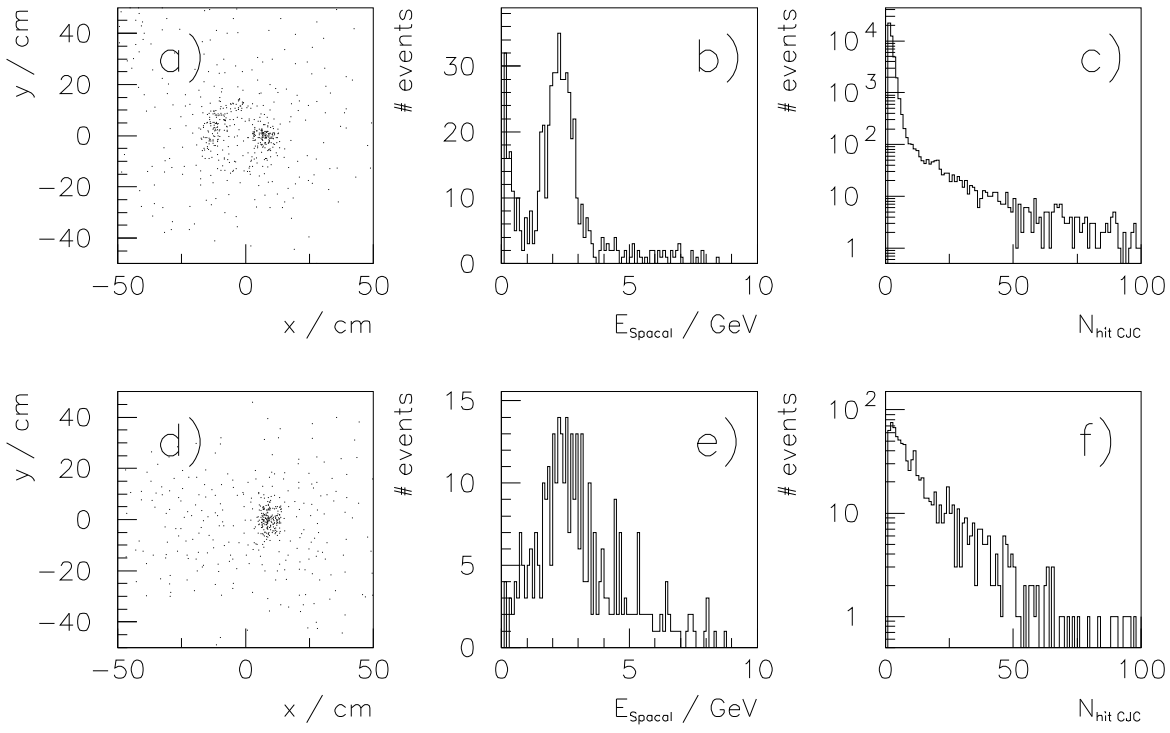

Figure 44: The location of energy depositions in the SpaCal during the November positron only run a) and in the MC d), the energy distribution of the "hot spot" at positive x in the data b) and Monte Carlo e) and the numbers of hits observed in the CJC in the data c) and Monte Carlo f) for all events.

4 Measures to combat background

4.1 Absorbers and collimators

4.1.1 Absorber at 11 m

As was discussed in [1], the flux of synchrotron radiation scattered back towards the H1 detector from the copper absorber at $z = -11$ m can be reduced by providing the absorber with a low albedo coating. Studies have shown that the originally proposed coating of silver and gold is problematic. It has proven impossible to solder a thin silver layer to the copper and attempts at electroplating have also failed. It is proposed that a layer of molybdenum be used instead. This will allow a reduction in the back-scattered synchrotron radiation flux by a factor of about 1.7, similar to that achievable with the silver and gold coating, and is technically much easier to realise. An additional gold layer would provide a further small improvement.

4.1.2 Modifications to collimator C5b

The tungsten collimator at $z = -1.5$ m, C5b, is designed to prevent backscattered synchrotron radiation from entering H1. Its current thickness of 20 mm is more than is necessary to shield the central detectors and, as was discussed in [1], the collimator provides a target in which particles produced in primary proton beam-gas interactions can re-scatter, causing backgrounds in the central chambers. Reducing the thickness of C5b reduces the amount of re-scattering and therefore the backgrounds in the H1 detector. The thickness of this collimator will therefore be reduced, but the design proposed in [1] will not be used as this has been shown to lead to significant HOM losses in this region. A new design, illustrated in figure 45, which has a significant taper to reduce HOM effects, is currently under investigation.

4.1.3 Shielding for the BST and CJC electronics

In [1] it was proposed that the BST electronics be shielded by surrounding the beam pipe inside the rear section of the BST with a 1 to 2 mm thick layer of lead. The purpose of the lead was to prevent synchrotron radiation causing damage to the electronics and this was thought to be worthwhile despite the slight increase in proton background that the lead will cause. Since this proposal, evidence has mounted that the radiation damage caused to the BST occurs in relatively few isolated incidents, typically partial beam losses during injection, against which the lead would offer no protection. The BST will be inspected in more detail early in the forthcoming shutdown. Only if these studies reveal that synchrotron radiation is responsible for the damage to the BST will the lead be installed. The design of the shielding would then be as shown in [1].

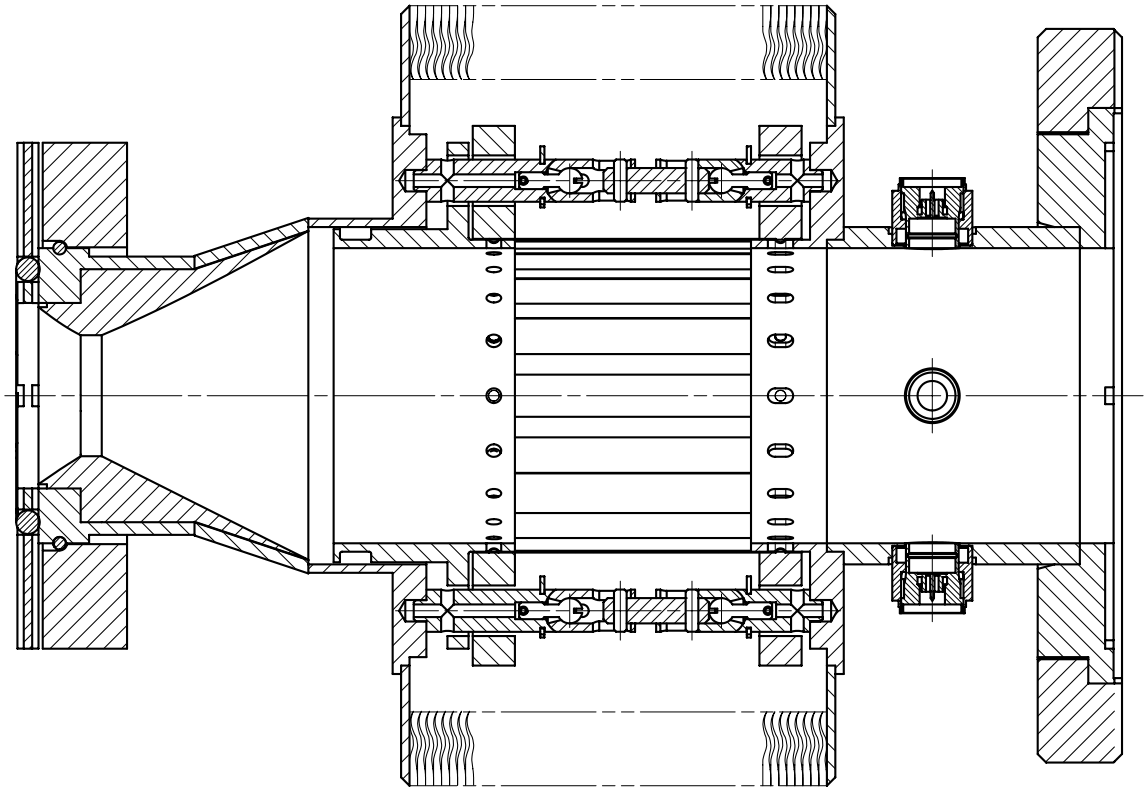

Figure 45: Proposed design of C5b collimator with taper to reduce HOM losses.

4.2 Pumps and instrumentation

4.2.1 Installation of a residual gas analyser

In order to allow monitoring of the residual gas composition close to the H1 interaction point during HERA running, it is proposed to install a mass spectrometer at $z = -3.6\,\mathrm{m}$. As is shown in figure 46, this can be achieved without compromising the physics acceptance of the H1 apparatus.

4.2.2 Installation of a getter pump

In order to improve the vacuum within the H1 experiment, it is proposed to install an ion getter pump at $z = -1.5\,\mathrm{m}$. A design has been developed that will allow the pump to be installed with minimal changes to the H1 apparatus, though aspects of the connection to the beam pipe are still under investigation. The particular concern is that adequate RF shielding must be provided to prevent possible HOM heating of the pump surfaces, which could lead to outgassing.

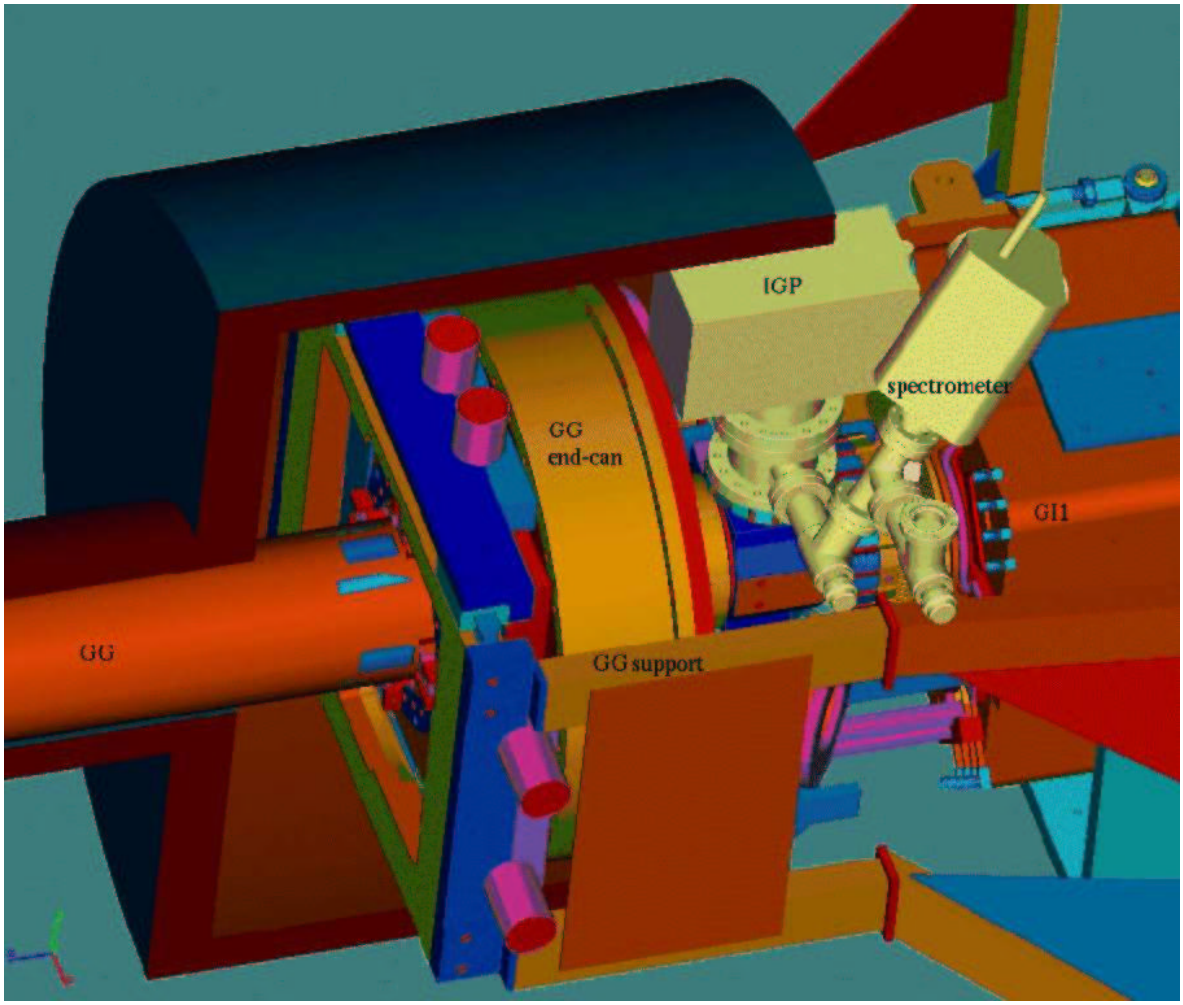

Figure 46: CAD drawing showing the installation of an ion getter pump and a mass spectrometer at $z = -3.6\,\mathrm{m}$ within the H1 detector.

5 Summary

The backgrounds within the H1 detector decreased significantly in the last quarter of 2002 and the quality and quantity of the data taken by H1 has increased accordingly. Problems remain, however, due to a combination of continuous background levels and background "spikes". A further reduction in the currents drawn in the CJC by a factor of about three is necessary if safe operation is to be possible with HERA design currents.

As described in this report, the understanding of the backgrounds within H1 is improving, though it is not yet complete. Measurements, some made using new instrumentation, and further simulations have shown that:

- The tighter acceptances and new magnet configuration following the luminosity upgrade imply that H1 is about 1.5 times more sensitive to backgrounds now than was the case during HERA I operation, section 2.1.
- The composition of the residual gas has not changed significantly as a consequence of the upgrade, section 2.2.
- The pressure in the interaction region is higher than prior to the upgrade and is more strongly dependent on the positron current. During the best running conditions achieved to date, the pressure was a factor of about 2 higher than that in 2000, section 2.3.
- The sensitivity of the H1 central detectors to the pressure in the HERA beam line has been determined as a function of the distance from the detector. Monte Carlo simulations and measurements are in reasonable agreement and imply that sensitivity extends to about 20 m along the proton beam line, section 3.1.
- Incidents in which the backgrounds are extremely high have caused damage to detectors close to the beam line, section 2.6.2.
- Heating of elements of the beam line in and around H1 through higher order mode losses at injection energies has been observed and has led to modifications in the design of some elements of the beam line, section 3.2.2.

Current extrapolations indicate that proton induced backgrounds will dominate at HERA II design currents. Improvements in the vacuum remain the primary means of reducing these. The following modifications are also foreseen:

- The coating of Absorber 4, probably with molybdenum.
- The alteration of the collimator C5b, with more emphasis now being placed on the reduction of higher order mode heating in this region, particularly during positron injection.
- The installation of an ion getter pump at $z = -1.5$ m.

Further, it is proposed to improve the instrumentation of the vacuum system by installing a residual gas analyser at $z = -3.6$ m.

Running H1 and HERA in a stable mode has led to valuable experimental data for first physics studies and for detector commissioning and calibration as well as to a deeper understanding of the sources of the background. During this process, operational procedures have been developed which are leading to more efficient data taking, especially regarding the improved vacuum conditions and the operation of the GO and GG magnets. It is essential that running be continued if the remaining questions regarding the background are to be adequately understood. For example, variations in the operating temperature of the GO and GG shields appear to significantly affect the vacuum and many aspects of this complex behaviour require further investigation, not least to determine whether the improvements observed in December are reproducible and to develop and test routine operational procedures regarding the GO and GG shield temperature and vacuum pump regeneration. Further, it is important that the spin rotators be tested before the shutdown to ensure that they do not introduce additional backgrounds and that polarisation can be achieved.

References

[1] H1 background working group, "Technical Report on the Beam Induced Backgrounds in the H1 Detector", H1 note H1-10/02-606, available from http://www-h1.desy.de/h1/www/publications/bgrep.pdf.

[2] J.C. Billy *et al*, "The LEP Vacuum System: A Summary of 10 Years of Successful Operation", Proc. of EPAC 2000, Vienna, Austria.

[3] M. Seidel *et al*, DESY MVA, private communication.

[4] M. Hoffman *et al*, DESY MPY, private communication.

[5] A. Antonov *et al*, ZEUS background working group, ZEUS-02-027.

[6] C.A. Miller, "Operating HERA as a Molecular Mass Spectrometer".